4-4-2018

Advanced Modeling, Design, and Control of ac-dc Microgrids

Hossein Saberi khorzoughi
Louisiana State University and Agricultural and Mechanical College, hosseinsaberi.kh@gmail.com

ADVANCED MODELING, DESIGN, AND CONTROL OF AC-DC MICROGRIDS

A Dissertation

Submitted to the Graduate Faculty of the
Louisiana State University and
Agricultural and Mechanical College
in partial fulfillment of the
requirements for the degree of
Doctor of Philosophy

in

The Department of Electrical and Computer Engineering

by
Hossein Saberi khorzoughi
B.Sc., Isfahan University of Technology, 2009
M.Sc., University of Tabriz, 2013
May 2018

ACKNOWLEDGEMENTS

I would like to express my gratitude to my advisor Dr. Shahab Mehraeen and all the committee members, Dr. Leszek S. Czarnecki, Dr. Mehdi Farasat, and Dr. Amin Kargarian, and also Dr. Jerry Trahan as the chair of Division of Electrical and Computer Engineering.

I also express gratitude to all ECE staff specially Ms. Beth Cochran for being always kind and helpful and would like to thank all my lovely friends at Louisiana State University who have been supportive throughout all my PhD study, especially Sharareh Heidarian and Hamed Shamkhalichenar. Finally, I am really grateful to my family for their invaluable support during all my study.

TABLE OF CONTENTS

ABSTRACT

An interconnected dc grid that comprises resistive and constant-power loads (CPLs) that is fed by Photovoltaic (PV) units is studied first. All the sources and CPLs are connected to the grid via dc-dc buck converters. Nonlinear behavior of PV units in addition to the effect of the negative-resistance CPLs can destabilize the dc grid. A decentralized nonlinear model and control are proposed where an adaptive output-feedback controller is employed to stabilize the dc grid with assured stability through Lyapunov stability method while each converter employs only local measurements. Adaptive Neural Networks (NNs) are utilized to overcome the unknown dynamics of the dc-dc converters at Distributed Energy Resources (DERs) and CPLs and those of the interconnected network imposed on the converters. Additionally, the use of the output feedback control makes possible the utilization of other measured signals, in case of loss of main signal, at the converter location and creates measurement redundancy that improves reliability of the dc network. The switching between measurement signals of different types are performed through using the NNs without the need to further tuning.

Then, in a small-scale ac grid, PV-based Distributed Generation (DG) units, including dc/dc converters and inverters, are controlled such that mimic a synchronous generator behavior. While other control schemes such as Synchronverters are used to control the inverter frequency and power at a fixed dc link voltage, the proposed approach considers both the dc-link voltage and the inverter ac voltage and frequency regulation. The dc-link capacitor stores kinetic energy similar to the rotor of a synchronous generator, providing inertia and contributes to the system stability.

Additionally, a reduced Unified Power Flow Controller (UPFC) structure is proposed to enhance transient stability of small-scale micro grids. The reduced UPFC model exploits dc link of the DG unit to generate appropriate series voltage and inject it to the power line to enhance transient stability. It employs optimal control to ensure that the stability of the system is realized through minimum cost for the system. A neural network is used to approximate the cost function based on the weighted residual method.

CHAPTER 1
RELIABLE OPERATION OF SMALL-SCALE INTERCONNECTED DC GRIDS VIA MEASUREMENT REDUNDANCY

1.1 Introduction

Renewable energy sources have attracted attention in modern power systems, as clean and abundant sources of energy. Distributed energy resources (DERs) such as Photovoltaics (PVs) and fuel cells generate dc power. Loads that consume dc power such as energy storage units, electronic loads, chargers, and LED lightings are increasingly used in the modern power system. Hence, employing a dc grid for interconnecting the DERs and loads can be more efficient since they are not challenged by frequency and phase stability and reactive power flow [1]-[5]. DERs are integrated into the grid through appropriate power electronics interfaces. Ac sources use an ac-dc interface to link to the dc grid whereas dc sources use dc-dc converters.

Unlike ac grids, dc networks studies are in their early stages. Several issues of dc systems need more attention and investigation. Stability of the dc grids is one important issue, specifically in small-scale interconnected dc grids with low inertia [6]-[7] that are more vulnerable to faults and disturbances. Constant-power loads (CPLs) can potentially cause instability and voltage collapse in dc grids. The negative resistance of the CPLs can destabilize the grid. Large oscillations or voltage collapse are observed in the presences of CPLs in dc grids without proper controls [8]. CPLs cause more deterioration specifically in low-inertia dc grids where only a small error margin between generation and consumption is allowed, and total load of the system is close to system generation limit. Stored energy in dynamic elements such as capacitors and inductors acts as system inertia [9]. However, it is not appropriate to increase the inertia by selecting overly larger dynamical elements due to practical limitations on the size of the components and an increased grid settling time. The intermittent nature of DERs also

threaten the stability of the small-scale grids. For instance, a passing cloud can decrease PV's output power abruptly and drastically. This along with the PV's nonlinear voltage-power characteristics adversely affects the system behavior.

In order to simultaneously regulate voltage of the grid and also optimize the power sharing between all dispatchable DERs a distributed control technique is presented in [10]. However, it does not address the small signal stability problems related to the nonlinear behavior of PVs and CPLs. In [11], authors proposed an optimized load sharing for different DGs through adjusting the droop gains. Droop-based schemes are known as decentralized control approaches that provide proper power sharing. In this method, the reference voltage of each converter is adjusted using virtual resistance R_{droop}. The proposed scheme offers desired current sharing and voltage regulation simultaneously using a Proportional Droop Index (PDI). Finally, the resultant reference voltage is applied using a PI controller. In [12]-[13] another improved droop mechanism is proposed that considers line resistances to achieve more precise power sharing. In addition, a variable droop gain is exploited for an accurate power sharing while preserving voltage regulation and power efficiency. In [14-18], authors proposed modified droop based methods to enhance load sharing between different sources. However, all these approaches incorporate conventional PI controllers to apply the desired voltage set points to the system. The PI controllers do not show promising performance in different conditions, specifically in the presence of CPLs in the grid [8].

In [19]-[22] load and source impedance "reshaping" have been proposed to enhance the stability margins. The small signal analysis is provided, and the stability of the system is evaluated for small variations around the operating point. The dc grid's stability using nonlinear

decentralized stabilization techniques are evaluated in [23]-[27]. Although large signal analysis are considered, a simple grid topology with single voltage level is studied, and interconnected dc grids with various bus voltages across the grid are not considered in these studies.

In [28], the Linear Quadratic Gaussian (LQG) method is employed where an extended Kalman filter is incorporated along with a Linear Quadratic Regulator (LQR). The CPL current is introduced as virtual disturbance, and the system response is composed of two parts: demand and disturbance responses. In [29], the only measured signal is the bus voltage where a Kalman filter is used to estimate the other states. However, it is shown that convergence rate of the Kalman filter adversely affects the performance of the controller. In order to stabilize a Medium Voltage dc (MVDC) network that feeds CPLs and resistive loads, linearization through state feedback is used in [30]-[31]. While in the majority of these works only a measured signal (output voltage) is utilized, and CPL stability problem is addressed, these schemes are proposed for a grid topology with a common dc bus that interlinks all the sources and loads and not an interconnected grid.

In [32], a nonlinear control method is proposed based on sliding mode control. The proposed scheme mitigates destabilizing effects of CPLs and provides an approximately fixed voltage for a dc bus. In [33], it is aimed to enhance stability of a dc grid consists of multiple dc-dc converters and CPLs. The proposed approach based on identifying the eigenvalues of the Jacobian matrix to stabilize the dc system. However, these methods are also applicable to a specific grid topology with single dc bus.

An output feedback control approach is presented in [34] for dc-dc buck converters. A reduced order observer is employed to estimate unmeasured states of the converter and stability

of the entire system is proved. Nonetheless, the proposed method is applied to a single converter in a centralized control manner and does not consider an interconnected network comprising different converters that affect each other.

The decentralized control is preferred in interconnected systems, where several loads and DERs interact [35]-[36], because it decreases data exchange, computational burden, and time delays while enabling easy addition of new DERs. In particular, nonlinear decentralized control schemes provide transient stability and steady-state performance using local measurements and offer larger stability margins in comparison with their linear counterparts. Distributed control mechanisms have been recently applied to the small-scale power networks; however, a communication infrastructure is required to collect global data from across the network [37].

In order to implement the control, the discrete-time models are desired [38]-[40] due to easier digital implementation and prevention of instability due to discretization of continuous-time systems. Conversely, most of the works in this area is based on continuous-time modeling [41]. Recent developments in this field by the author includes [42]-[44] that use state- and output-feedback methods. In these works, the nonlinear characteristics of both the DERs (PVs) and CPLs are taken into account. The CPLs are built as resistive loads that are connected to the grid via dc-dc converters and controlled such that absorb constant power. Both DER and CPL converters are controlled by the proposed decentralized nonlinear controllers. Then, through the Lyapunov stability method the stability of all the converters' states in the dc grid is proven. When using output feedback controller, the other available converter states can be potentially used to provide measurement redundancy. However, this was not studied in the previous work [44].

In this paper, two major improvements are proposed over the authors' previous work. First, using output-feedback decentralized controller, the additional available states are used for control when the main measurement is lost. It is proven that the states can be utilized with no change in the nonlinear controller structure or parameters with assured overall grid stability. Second, the proposed output-feedback fault tolerant controller is implemented in the hardware using a 1400W dc circuit that includes three photovoltaic sources, one CPL, and seven resistive loads. The IEEE 14-bus network topology is chosen to establish an interconnected network. Adaptive neural networks (NNs) [45]-[47] are employed to overcome the unknown dynamics of the dc-dc converters at DERs and CPLs and to stabilize the entire grid. The approximation property of the neural networks can effectively replace the unknown dynamics of converters and those of the interconnected network imposed on the converters. The dc grid interconnects distributed energy resources, CPLs, and resistive loads, and the control approach is not restricted to any specific topology. Additionally, it should be noted that the goal of this work is short-term stability enhancements that lie in the microgrid primary control [48].

The rest of this chapter is organized as follows. The dc grid topology is presented in section 2. In Section 3, nonlinear discrete-time decentralized model of photovoltaic DER is explained and the CPL model is developed in Section 4. The simulation and experimental results on the low-voltage small-scale dc grid are given in Section 5. Section 6 includes the concluding remarks of the work.

1.2 Interconnected DC Grid

Different types of DERs can be used as low inertia power sources in a small scale dc grid. Without loss of generality, PV units are selected as the DERs that are connected to the grid via

dc-dc buck converters. Resistive loads are connected to the grid directly while CPLs are tied to the grid via dc-dc buck converters as shown in Fig. 1.1. The CPL converter keeps the voltage constant across a resistive load such that the power consumption at the CPL bus remains constant regardless of dc grid voltage. Nonetheless, any type of load that interact with the grid as a CPL, such as induction motors that are connected to the dc grid via dc-ac converters, can be stabilized using the proposed control scheme.

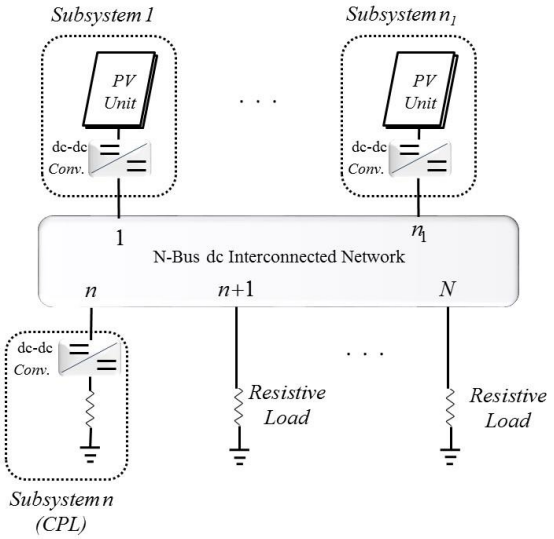

Fig. 1.1 Interconnected dc Network

Although the boost converter poses higher output voltage, due to the stability issues, the buck converter is more reliable for the PV system. For increasing the voltage level, transformers at the ac side or topologies like forward converters that employ transformers can be used, without affecting stability of the system [49]. Overall, any converter can be modeled more or less the same way as the buck converter chosen here. This work aims at design of stabilizing controllers that control the output voltages with any available converter signal as opposed to [44] to achieve tolerance against loss of measurement. The nonlinear buck converter models are used

and duty cycle control is performed via nonlinear decentralized neural network-based adaptive controller. The proposed controller employs an observer to estimate the unmeasured local states. The dc-dc converters of DERs and CPLs are explained in [43] and [44] and is briefly reviewed in the next section.

1.3 DER and CPL Model Development

The DERs and CPLs are connected to the grid through dc-dc buck converters. In this section, first a DER converter model is developed and then, a model is presented for CPL converter n_1.

A. DER Converter Model

The dc-dc converter that ties the DER to the grid is shown in Fig. 1.2. Index i represents the converter number. If $1 \le i \le n_1$, it refers to a DER converter, and if $n_1 < i \le n$, a CPL converter is denoted. The input-output canonical equations in discrete domain for the converter model is derived. The state variables of the DER converter are input voltage $v_{in,i}$, inductor current $i_{L,i}$, and output voltage $v_{out,i}$ as depicted in Fig. 1.2. Only one state (such as $v_{out,i}$) is utilized in the control while the other measured states provide measurement redundancy. The dynamical equation of the DER converter in discrete domain at time step kT is written as [43]

$$
\begin{aligned}
v_{in,i}((k+1)T) &= C_{in,i}^{-1}\left[\int_{kT}^{(k+1)T} i_{1,i}(t)\,dt - \int_{kT}^{(k+D_i)T} i_{L,i}(t)\,dt\right] + v_{in,i}(kT) \\
i_{L,i}((k+1)T) &= L_i^{-1}\left[\int_{kT}^{(k+D_i)T} v_{in,i}(t)\,dt - \int_{kT}^{(k+1)T} v_{out,i}(t)\,dt\right] + i_{L,i}(kT) \\
v_{out,i}((k+1)T) &= C_{out,i}^{-1}\int_{kT}^{(k+1)T} (i_{L,i}(t) - i_{2,i}(t))\,dt + v_{out,i}(kT)
\end{aligned}
\tag{1}
$$

where T is the converter switching period, D_i is duty cycle, L_i is the converter's inductor, $C_{in,i}$ and $C_{out,i}$, are the input and output capacitances, $i_{1,i}$ and $i_{2,i}$ are input and output currents and k is the discrete step ($k \in Z^+$). The injected input current $i_{1,i}$ is a function of PV voltage.

The state error vector is defined as $\bar{X}_i(k) = X_i(k) - X_{o,i} = [\bar{v}_{in,i}(k), \bar{i}_{L,i}(k), \bar{v}_{out,i}(k)]^T$ with $X_i(k) = [v_{in,i}(k), i_{L,i}(k), v_{out,i}(k)]^T$ and $X_{o,i}$ is the steady-state vector. Input and output current errors are $\bar{i}_{1,i}(k) = i_{1,i}(k) - I_{1,i}$ and $\bar{i}_{2,i}(k) = i_{2,i}(k) - I_{2,i}$ where $I_{1,i}$ and $I_{2,i}$ are steady-state input and output currents.

The control objective is to make the converter measured state error zero by generating an additional duty cycle $\bar{D}_i(k)$ to the steady-state duty cycle $D_{o,i}$ where $D_i(k) = D_{o,i} + \bar{D}_i(k)$. Hence, the converter state is stabilized around its reference value after grid disturbances and faults have cleared.

Remark 1. The converter duty cycle reference can be set by the upper level control in the grid (power sharing controller). Short term stability (less than second) is the goal here and thus slower system dynamics such as slow cloud effects or load changes are not considered. Due to faster dynamics considered in the proposed control method set point $D_{o,i}$ can be considered constant.

It is notable that system (1) is in a highly nonlinear form and thus must be converted to Brunovski canonical form [50], before any known control mechanism can be applied.

$$\begin{aligned} x_1(k+1) &= x_2(k) \\ x_2(k+1) &= f(x) + g(x)u \end{aligned} \tag{2}$$

However, the Brunovski canonical model depends on the selected measured output state; i.e., the order and the value of coefficients in the model varies when the target output state varies ($v_{in,i}$, $i_{L,i}$, or $v_{out,i}$). This is important to note when switching from one measured state to another during measurement failures in a redundancy-supported control mechanism. For simplicity, one can conclude from the linearized form of system (1), shown in (2), to see this variation but the actual controller design will be conducted using the original nonlinear forms (1):

$$\begin{aligned} v_{in,i}((k+1)T) &= T/C_{in,i} \times [i_{1,i}(kT) - D_i\, i_{L,i}(kT)] + v_{1,i}(kT) \\ i_{L,i}((k+1)T) &= T/L_i \times [D_i\, v_{in,i}(kT) - v_{out,i}(kT)] + i_{L,i}(kT) \\ v_{out,i}((k+1)T) &= T/C_{out,i} \times [i_{L,i}(kT) - i_{2,i}(kT)] + v_{out,i}(kT)\,. \end{aligned} \tag{3}$$

From (3), one can observe that selecting output voltage $v_{out,i}$ leads to a second-order system whereas input voltage $v_{in,i}$ or inductor current $i_{L,i}$ render first-order systems. Similar conclusion applies to (1).

In addition, the output current $i_{2,i}$ in (1) depends on the unavailable states of other converters (due to decentralized nature of the control). This current appears only when $v_{out,i}$ is selected as the measured output. Output current $i_{2,i}$ reflects the effect of the entire network on the individual DER converter and is sometimes called an *interconnection* term and will be discussed later.

For convenience, it can be assumed that the converter model is a second-order dynamical system so that one can include different systems (first- and second-order systems) when different measured outputs are selected. Note that a first-order dynamical system can be converted to

second-order one by adding an integrator; i.e., adding the delayed state as a new state. Once the system is available in second-order dynamical form the nonlinear decentralized controller can be developed and is explained next.

For simplicity, the controller development is described for DER measured output voltage, which is a second-order system but the approach can be applied to the other measured states, similarly.

State-space equations (1) can be converted into general decentralized form when choosing output voltage error as the output of the converter $y_i(k) = e_{1,i}(k) = \bar{v}_{out,i}$ and defining the dynamic $e_{1,i}(k+1) = e_{2,i}(k)$. Next, dynamic $e_{2,i}(k+1)$; i.e., output voltage error $\bar{v}_{out,i}(k+2)$, is obtained using the approach presented in [43] as

$$\begin{aligned} e_{1,i}(k+1) &= e_{2,i}(k) \\ e_{2,i}(k+1) &= f_i(\bar{X}_i(k)) + g_i(\bar{X}_i(k))u_i(k) + \Delta_i(e(k)) \end{aligned} \tag{4}$$

for $1 \le i \le n_1$ where $u_i(k) = \bar{D}_i(k)$ is the converter duty cycle error (input to the converter), $y_i(k) = e_{1,i}(k)$ is the only converter state that is used for control, $f_i(\bar{X}_i(k))$ and $g_i(\bar{X}_i(k))$ are unknown nonlinear functions that originate from system (1) nonlinearities, and $\Delta_i(e)$ characterizes unknown nonlinear dependency of output current $\bar{i}_{2,i}(k)$ to other converters' states. Function $\Delta_i(e(k))$ depends on the entire system's state vector $e(k) = [e_1(k), \ldots, e_n(k)]^T$ with $e_i = [e_{1,i}, e_{2,i}]^T$ for $1 \le i \le n$ and is the *interconnection* term that is a function of all the converters' states including the DERs and CPLs. DER state errors e_i (for $1 \le i \le n_1$) are presented in (4) while state errors of the CPL e_i (for $n_1 < i \le n$) will be given in the

following section. Note that when input voltage $v_{in,i}$ or inductor current $i_{L,i}$ are selected, the DER model resembles

$$\begin{aligned} e_{0,i}(k+1) &= e_{1,i}(k) \\ e_{1,i}(k+1) &= f_i(\bar{X}_i(k)) + g_i(\bar{X}_i(k))u_i(k)) \end{aligned} \tag{5}$$

where $e_{0,i}(k) = e_{1,i}(k-1)$ is the integrator (delay) in discrete-time. Model (5) can be easily represented as model (4) with zero interconnection effect. Also, a new set point for the created delayed state (measured state error) must be defined. One can conveniently choose zero as the set point, noting that $v_{in,i}$ or $i_{L,i}$ errors are zero at steady state.

Remark 2. Output feedback control system is aimed here and requires only one measured output in the proposed scheme. Note that there are three states, which can be measured and used for DER control. However, the developed dynamical model is of order one ($v_{in,i}$ or $i_{L,i}$) or two (for $v_{out,i}$) leaving two or one of the states unobservable, respectively. The unobservable states are often called zero states and must be assured to be stable once the observable state is proven stable. Once the proposed adaptive controller assures stability of the observed states, due to properties of currents and voltages in the dc network the unobservable states cannot be unbounded [See 42 and 43]. In addition, the interconnection effect appears for state dynamic $\bar{v}_{out,i}$ while it is zero for the others ($\bar{v}_{in,i}$, $\bar{i}_{L,i}$) for which the interconnection effect appears in the zero dynamics. However, since the control mechanism is applied to all the DER and CPL converters, all observed states in the network are stable and thus the unobservable states remain stable due to inherent limitations that exist for states of the dc circuit as explained earlier. Thus, one must prove that the observable states of all converters in the network are stable simultaneously.

Remark 3. The presented model can utilize one of the three available converter states. In practice measuring all three converter states are not very expensive, and thus, the three measurements are available. Since the presented model relies on only one output measurement, the other two measurements provide redundancy and can be used when the original measured signal is lost, keeping the converter system up and running inside the control loop with no change in the controller parameters due to using and adaptive neural network controller as will be explained.

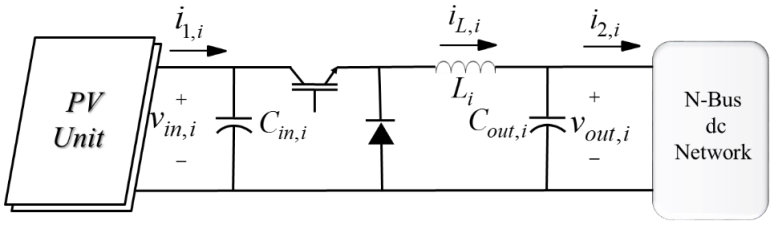

Fig. 1.2 dc-dc buck converter

B. Constant-power Load's Converter Model

The dc grid feeds the constant-power and resistive loads. Resistive loads are connected to the network buses directly while CPLs are connected via dc-dc buck converters that provide constant power for the load. The dc-dc buck converter is the interface between the dc bus and the load and keeps the voltage across the load resistance constant. Thus, the absorbed power at the dc bus remains constant regardless of grid voltage variations. The input voltage is the bus voltage and the output voltage of this converter is voltage across the load, as shown in Fig. 1.3.

Remark 4. The CPL mechanism is different from that of the DER in two ways. First, the input current $\bar{i}_{1,i}(k)$ is a function of the grid voltage and thus a function of the entire grid state vector. It reflects the *interconnection* effect. Second, the output current $\bar{i}_{2,i}(k)$ is only dependent on $\bar{v}_{out,i}(k)$ and is not an interconnection term in CPL. These are just the opposite in DER.

Similar to DER converter, the state error vector is defined as $\bar{X}_i(k) = X_i(k) - X_{o,i} = [\bar{v}_{in,i}(k), \bar{i}_{L,i}(k), \bar{v}_{out,i}(k)]^T$

with $X_i(k) = [v_{in,i}(k), i_{L,i}(k), v_{out,i}(k)]^T$ and $X_{o,i}$ as the steady-state vector. Also, input current error is $\bar{i}_{1,i}(k) = i_{1,i}(k) - I_{1,i}$ and the output current is defined as $\bar{i}_{2,i} = \bar{v}_{out,i} / R_{L,i}$.

A third order system can be obtained for CPL converter similar to that of the DER converter described in (3) [43]. In addition, similar arguments to Remark 4 can be brought here to show that the choice of measured output can change resulting system order leading to a maximum second-order system and that the interconnection term can appear in either observable state dynamics or zero states' (unobservable dynamics). This discussion is skipped here due to similarity to the DER case. Consequently, one can propose a converter second-order description as

$$e_{1,i}(k+1) = e_{2,i}(k) \quad for \quad n_1 + 1 \le i \le n$$

$$e_{2,i}(k+1) = f_i(\bar{X}_i(k)) + g_i(\bar{X}_i(k))u_i(k) + \Delta_i(e(k)) \tag{6}$$

where $u_i(k) = \bar{D}_i(k)$ is the converter duty cycle error and $\Delta_i(e(k))$ is the interconnection effect that can be zero for some choice of measurement.

So far, decentralized canonical forms for both DER and CPL converters are explained. The proposed decentralized output-feedback controller is explained in the next section.

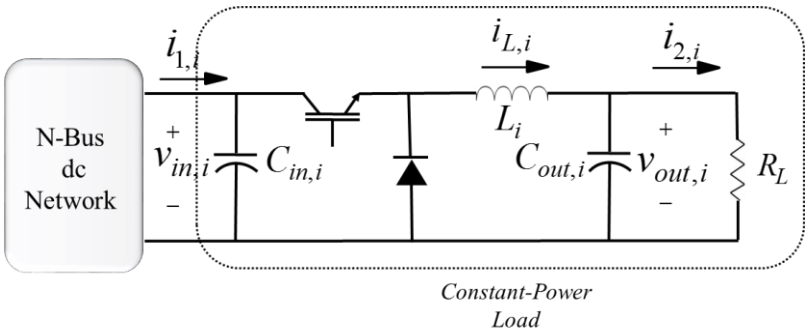

Fig. 1.3 Constant-power load dc-dc buck converter.

1.4 Decentralized Output-Feedback Controller Design

In the rest of the paper, system model (3) is employed to denote both DER and CPL converter models. The decentralized output-feedback controller introduced in [43] is applied to system model (3), using knowledge of only one of the states. The control objective is to stabilize error $e(k)$ at the origin ($e=0$). Since only one measurement is utilized ($e_{1,i}$ for all $1 \le i \le n$), an observer is utilized to estimate other states of the system. Two assumptions and one definition are needed prior to design of the output-feedback controller.

Assumption 1- In the small-scale system, functions $g_i(\overline{X}_i(k))$ satisfies

$$0 < g_{i,\min} \le g_i(\overline{X}_i(k)) \le g_{i,\max} \tag{7}$$

where $g_{i,\min}$ and $g_{i,\max}$ are positive constants. It should be noted that $v_{in,i}$ (DER interface voltage) have maximum value. Also, it is reasonable to assume that solar voltage $v_{in,i}$ stays away from zero. Since g_i is a function of $v_{in,i}$ and some other limited parameters of the system, (7) is a realistic assumption [43].

Assumption 2 [51]- The interconnection terms are bounded by a function of the entire grid states such that $\Delta_i(e) \le \sigma_{0i} + \sum_{j=1}^{N} \eta_{ij} \|e_j\|$ where σ_{0i} and η_{ij} are positive constants for $1 \le i \le n$. This assumption is valid for dc small-scale grids [43].

A. Observer Design

Neural networks (NNs) approximate general nonlinear functions $f(X) = W^T \varphi(V^T X) + \varepsilon$ [52] where φ is the activation function, W is the ideal (target) weight matrix, and ε is the functional reconstruction error. The unknown states of the DER and CPL converters in (6) are approximated through neural network (7) as

$$e_{2,i}(k) = f_i(\bar{X}_i(k-1)) + g_i(\bar{X}_i(k-1))u_i(k-1) = W_{1,i}^T \varphi_i(V_{1,i}^T M_i(k-1)) + \varepsilon_{1,i}(M_i(k-1)) \quad (8)$$

where $M_i(k-1) = [e_{1,i}(k-1), e_{2,i}(k-1), u_i(k-1)]^T$ for all $1 \le i \le n$. While the ideal weights, reconstruction error, and converter states are not available, estimations of the NN weights and converter states are used in the observer:

$$\begin{aligned} \hat{e}_{1,i}(k) &= \hat{e}_{2,i}(k-1) \\ \hat{e}_{2,i}(k) &= \hat{W}_{1,i}(k-1)\varphi_i(V_{1,i}{}^T \hat{M}_i(k-1)) \end{aligned} \quad (9)$$

where $\hat{e}_i = [\hat{e}_{1,i}, \hat{e}_{2,i}]^T$ is the estimation of e_i and $\hat{M}_i(k-1) = [\hat{e}_{1,i}(k-1), \hat{e}_{2,i}(k-1), u_i(k-1)]^T$ is estimated for $M_i(k-1)$ for all $1 \le i \le n$. Also, $\hat{W}_{1,i} \in R^{L_{1,i} \times 1}$ is the approximation of target neural network weight matrix $W_{1,i}$ with $L_{1,i}$ the number of the hidden layer neurons, and $\varphi_i(.)$ is the neural network activation function vector. The hidden layer weight matrix $V_{1,i}$ is randomly chosen at the first and kept constant [53]. For simplicity $\varphi_i(V_{1,i}{}^T M_i(k-1))$ and $\varphi_i(V_{1,i}{}^T \hat{M}_i(k-1))$ are shown by $\varphi_i(k-1)$

and $\hat{\phi}_i(k-1)$, respectively. As the converters' neural network target weight matrices are unknown, an update law is assigned to find observer NN weights (beginning with an initial estimation) as

$$\hat{W}_{1,i}^{T}(k) = \hat{W}_{1,i}(k-1) - \alpha_{1,i}\hat{\phi}_i(k-1) \times [\hat{W}_{1,i}^{T}(k-1)\hat{\phi}_i(k-1) + l_{1,i}\,\tilde{e}_{1,i}(k-1)] \tag{10}$$

where $0 < \alpha_{1,i} < 1$ and $l_{1,i} < 1$ are user defined positive constants and $\tilde{e}_i = \hat{e}_i - e_i$ is the state estimation error. Then, the decentralized output-feedback controller can be developed.

B. Controller Design

Here, a controller will be developed to stabilize converter model (4) using the estimated states of observer (9). Since the models include unknown dynamics (*f* and *g*), another neural network is incorporated for approximating the unknown dynamics.

The error dynamic of the system is written as $e_{m,i}(k+1) = f_i(\bar{X}_i(k)) + g_i(\bar{X}_i(k))u_i(k) + \Delta_i(e(k))$. One may aim a behavior such as $e_{2,i}(k+1) = K_i g_i(\bar{X}_i(k))e_{2,i}(k)$ with $K_i g_i(\bar{X}_i(k)) < 1$ to attain asymptotically stable dynamic for the error when there is no grid effect Δ_i; hence, ideal stabilizing control input for model (4) can be defined as $u_{d,i} = -g_i(\bar{X}_i(k))^{-1}(f_i(\bar{X}_i(k)) + K_i e_{2,i}(k))$ where K_i is a positive design constant. Nonetheless, practically, the internal dynamics $f_i(\bar{X}_i(k))$ and control gain $g_i(\bar{X}_i(k))$ are unknown and $u_{d,i}$ is not available. Thus, the neural network function approximation property is utilized to approximate $u_{d,i}$ as

$$u_{d,i} = W_{2,i}^{T}\rho_i(V_{2,i}^{T}Y_i(k)) + \varepsilon_{2,i}(V_{2,i}^{T}Y_i(k)) + K_i e_{2,i}(k) \tag{11}$$

where $W_{2,i}$ is an unknown target NN weight matrix, $Y_i(k) = [e_{1,i}(k), e_{2,i}(k)]^T$, and $\varepsilon_{2,i}(.)$ is the NN function approximation error for all $1 \le i \le n$. Since $W_{2,i}$, $\varepsilon_{2,i}$, and the full converter state

vector $e_i(k)$ are not available, $u_{d,i}$ is developed by means of approximate NN weights along with the estimated converter states through nonlinear observer (9); that is,

$$u_i = \hat{u}_{d,i} = \hat{W}_{2,i}^T \rho_i (V_{2,i}^T \hat{Y}_i(k)) + K_i \hat{z}_{m,i}(k) \tag{12}$$

where $\hat{W}_{2,i}$ is the NN weight estimation matrix and $\hat{Y}_i(k) = [\hat{e}_{1,i}(k), \hat{e}_{2,i}(k)]^T$. Similar to the observer case, the hidden layer weight matrix $V_{2,i}$ is chosen initially at random and kept constant. Since NN weights are to be estimated, define the controller NN weight update law as

$$\hat{W}_{i2}(k+1) = \hat{W}_{i2}(k) - \alpha_i \hat{\rho}_i(k)[\hat{W}_{i2}^T(k)\hat{\rho}_i(k) + l_{i2}e_{i1}] \tag{13}$$

where $0 < \alpha_{2,i} < 1$ and $l_{2,i} < 1$ are user defined positive constants and $\rho_i(V_{2,i}^T \hat{Y}_i(k))$ is shown by $\hat{\rho}_i(k)$ for simplicity. The stability of the nonlinear discrete-time interconnected system (3) is proven and given in [44]. The errors $e_i(k)$, the state estimations errors $\tilde{e}_i(k)$, and NN weight estimation errors $\tilde{W}_{i1}(k)$ and $\tilde{W}_{i2}(k)$ of the individual converters are stable and bounded in the presence of unknown dynamics $f_i(\overline{X}_i(k))$, control gain matrix $g_i(\overline{X}_i(k))$, and interconnection terms $\Delta_i(e)$ for $1 \le i \le n$ (See proof in [44]). Fig. 1.4 depicts the entire control system block diagram that is composed of the adaptive observer and controller.

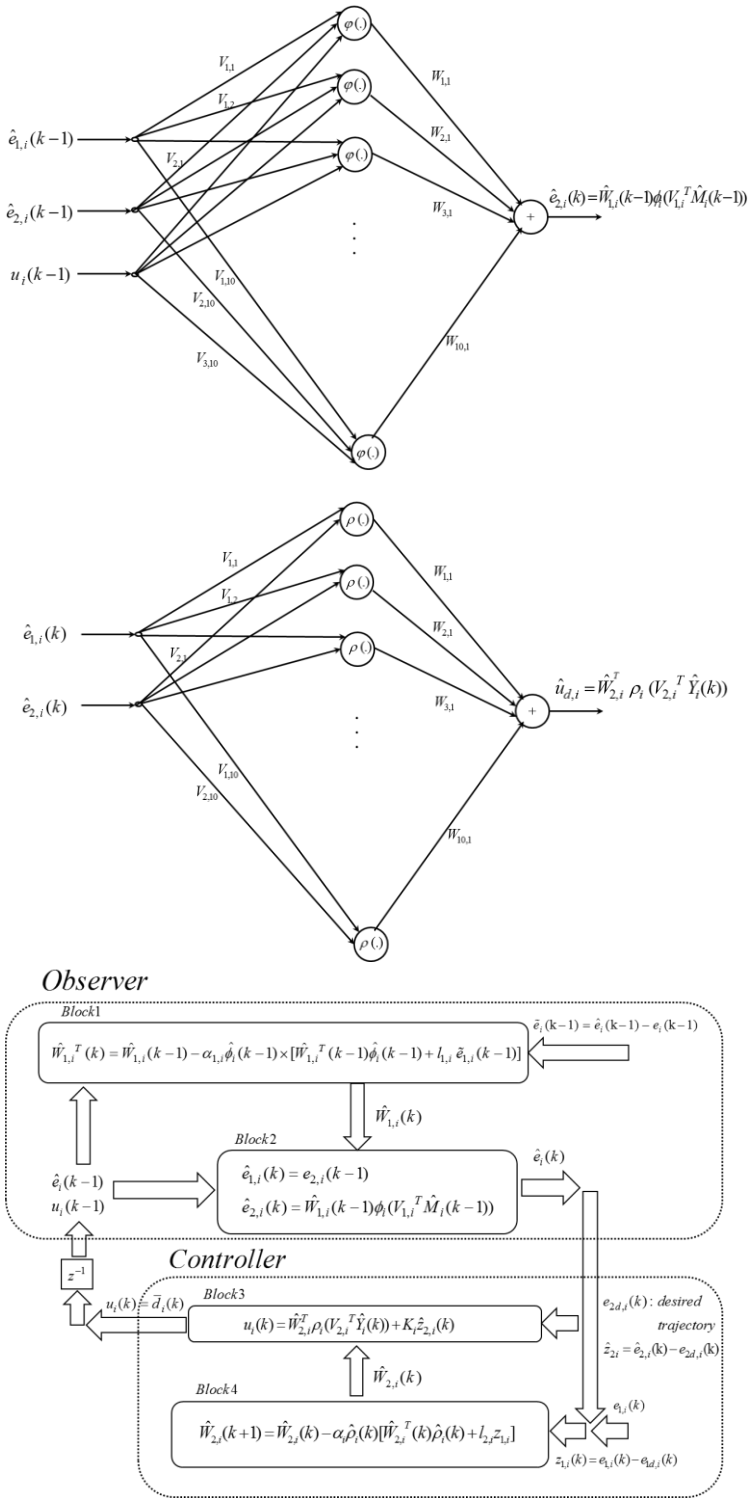

Fig. 1.4. Observer neural network, controller neural network, and adaptive output feedback controller block diagram

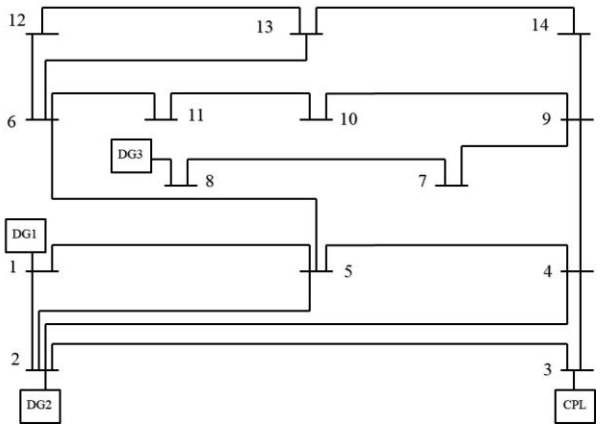

Fig. 1.5. Test system based on IEEE 14-bus topology

1.5 Simulation and Hardware Test Results

In order to verify efficiency of the proposed decentralized output-feedback controller, simulations and hardware experiments are carried out in Matlab/Simulink environment as well as on a lab setup. The test system is a dc network developed based on IEEE 14-bus topology shown in Figs. 1.5. Three PV units are connected as the DERs in the network while loads include one CPL and a number of resistive loads that are directly connected to the network buses. Lines are series RL components with a nominal grid voltage of 48V. The DER and CPL controllers stabilize the output voltages at their nominal values in the presence of disturbances in the network. The network specifications are given in Table 1.1. An experimental prototype is built to examine the performance of the proposed scheme (Fig. 1.6). Six 280W, 39.5V solar panels are used to build three solar DERs (two panels in series per DER). dSPACE Microlabbox control platform is used to apply the control method using MATLAB. The control signals are generated by the Microlabbox PWM unit and routed to the optocoupler interface board. The interface board provides proper signals to run the IGBTs' drivers that in turn run the IGBT switches. The switch modules include IGBTs and diodes, configured such that form dc-dc buck converters. Input

capacitors ($C_{in,i}$) are connected to the switches input terminals and the inductors (L_i) tie the converters to the grid buses that are connected together through R-L lines. Output capacitors and local loads at the converters' output terminals are in the lower part where the measurement board is also mounted to obtain the locally measured signal of each converter. The measured signals are sent to the control platform via MicrolabBox ADC channels.

Table 1.1. System parameters

Parameter	Value	Parameter	Value
- PV short circuit current	I_{sc} =9.71 A	$P_{L,1}$	100W-Resistive
- PV open circuit voltage	V_{oc} =39.5 V	$P_{L,2}$	100W-Resistive
- PV maximum power	V_{oc} =280 W	$P_{L,3}$	100W-CPL
- Conv. capacitors	C_{in}=300, C_{out}=300 μF	$P_{L,4}$	100W-Resistive
- Conv. inductance	L=20 mH	$P_{L,5}$	100W-Resistive
- Switching frequency	f_s=10 kHz	$P_{L,6}$	100W-Resistive
- Line resistances	R_{Line}= 0.3 Ohm	$P_{L,7}$	100W-Resistive
- Line inductances	L_{Line}= 0.3 mH	$P_{L,8}$	100W-Resistive
- CPL conv. capacitors	C_{in}=0.1, C_{out}=0.1 mF	$P_{L,9}$	100W-Resistive
- CPL conv. inductance	L=10 mH	$P_{L,10}$	100W-Resistive

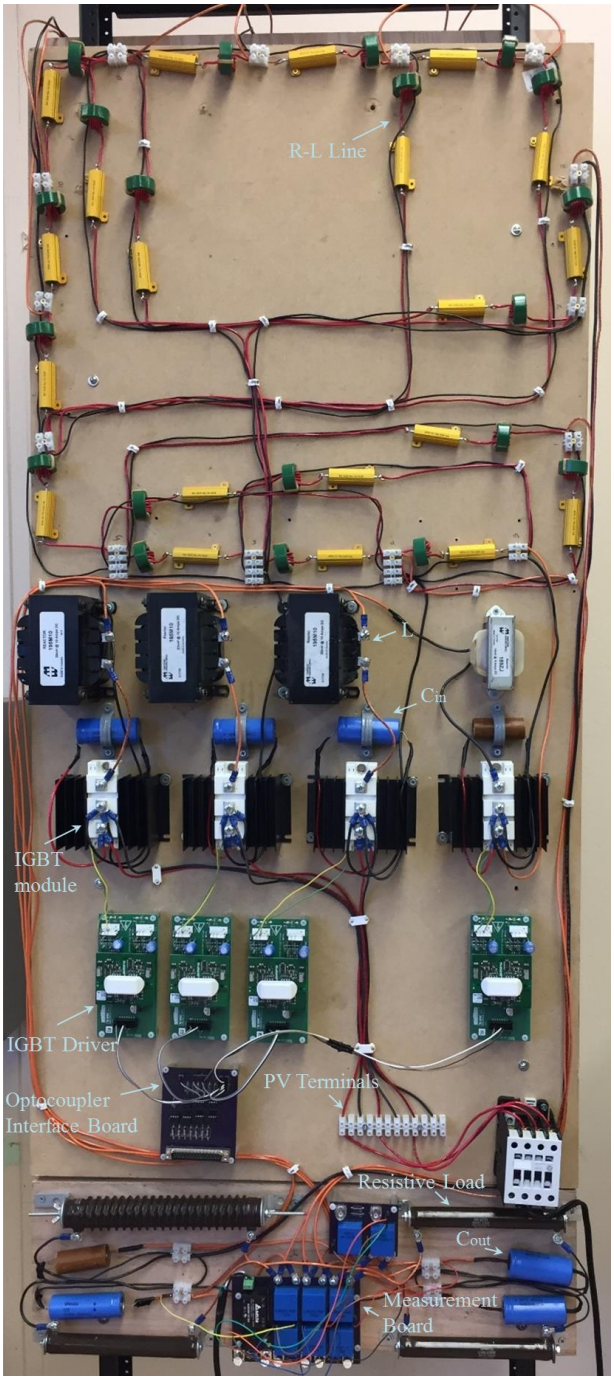

Fig. 1.6 Implemented dc grid

Various scenarios are examined to ensure effectiveness and robustness of the proposed control scheme. It should be noted that for better stability all PV units are operating in the stable

operation zone where $v_{in} > V_{MPP}$; thus, in order to increase the PV delivered power, voltage at the PV terminal (input voltage) must decrease.

Neural networks are utilized to approximate unknown dynamics $f(X) = W^T \varphi(V^T X) + \varepsilon$ adaptively, as explained in Section 4. The number of hidden layer neurons in matrix V can be increased to improve the approximation precision; however, it is limited to 10 neurons in all DER and CPL controllers to minimize computational burden. The controllers are tuned for the three measurements (DDC output voltage, input voltage, and inductor current) initially and kept unchanged throughout all the following experiments as described in Table 1.2. The controllers need not be altered when disturbance scenarios change due to adaptive nature of the proposed decentralized controller.

Table 1.2. Controllers parameters

NN Controller Parameters		PI Controller Parameters	
K	0.9	K_p	20
l_1	0.5	K_I	50
l_2	0.1		
α	0.1		

Case 1- CPL sudden load change: In this hardware-simulation experiment, the CPL at bus 3 is stepped up to 120W from nominal value of 80W. The DER controllers measure output voltage and adjust the converters duty ratios to maintain grid voltage at nominal values by extracting more power out of the PV units, while the CPL controller provides a constant voltage over the resistive load. Bus 1 voltage ($v_{out,1}$) and CPL voltage ($v_{out,3}$) are depicted in Fig. 1.7. In addition, generated power of the DER #1 (Bus 1) and power consumption at CPL bus (Bus 3) are demonstrated. From Fig. 1.7 voltages are controlled satisfactorily around the nominal values. Moreover, the increased demand of the CPL resulted in additional DER power generations;

however, only one DER power is illustrated here. Simulation results and experimental ones reasonably match according to the figures.

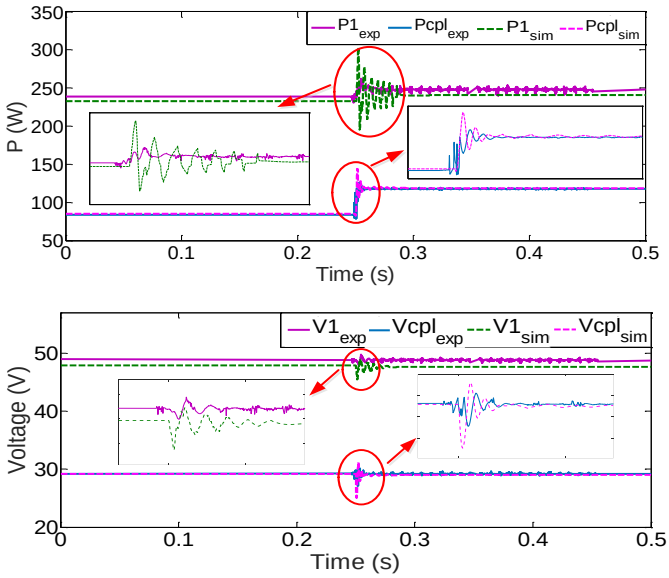

Fig. 1.7 Case 1: DER delivered power at bus #1 and CPL absorbed power (located at bus #3) as well as voltage at bus #1 and CPL output voltage (v_{out1} and v_{out3}) during CPL power step change (index *sim* denotes simulation results, while index *exp* denotes experimental results).

Case 2- Loss of generation: In this simulation scenario, the PV unit at bus 2 is disconnected from the grid for 0.1 second from t=0.9s to t=1s. While the DER generation at bus 2 is interrupted, the other DERs compensate the power loss to keep the voltage of the grid at the nominal value. The input and output voltages as well as the injected power of the DER at bus 2 is shown in Fig. 1.8 in comparison with the PI controllers' performance that shows the proposed method efficiency in regulating the voltage in the sudden absence of one of the generation units using the measured output voltage. It should be noted that the other sources compensate loss of generation at one of the buses and maintain the grid voltage. In contrast, the PI controllers cannot retrieve the pre-fault conditions using the measured output voltage.

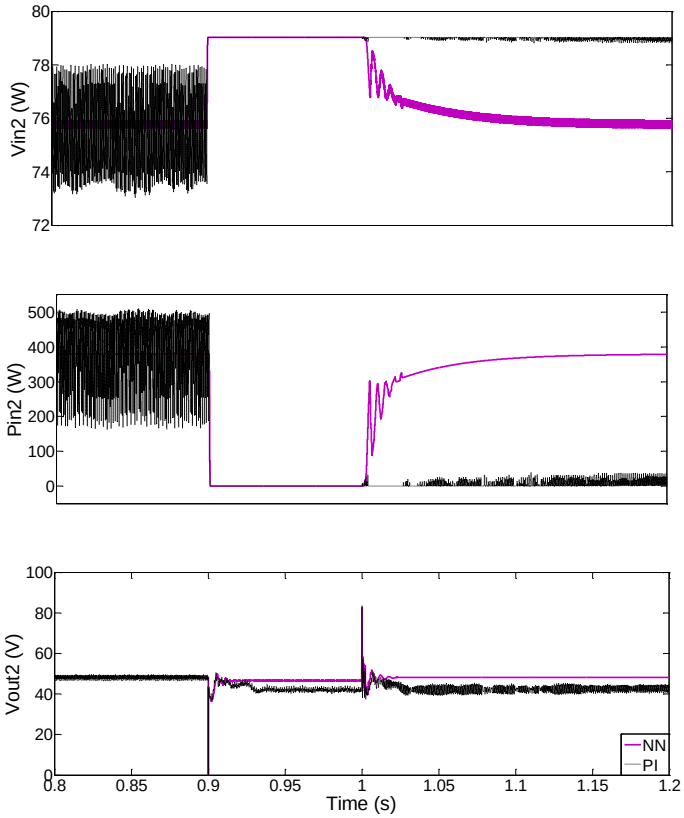

Fig. 1.8 Case 2: Proposed controller's performance is compared to that of the PI controller's when DER #2 is interrupted for 0.1s. The proposed controller is able to retrieve the generation.

Case 3- Loss of generation: In this next hardware experimental study, the DER power generation at bus 1 is interrupted for 0.5 second while the output voltage is the utilized measured signal of all converters. In absence of one generation unit, the other sources compensate the loss of power at bus 1 and keep the voltage of the grid and CPL output voltage at their nominal values as demonstrated in Fig. 1.9. Due to sudden reduction of generation at bus 1, the voltage variations are more severe in this case in comparison with the previous case (passing cloud) that exhibited slower rate of change.

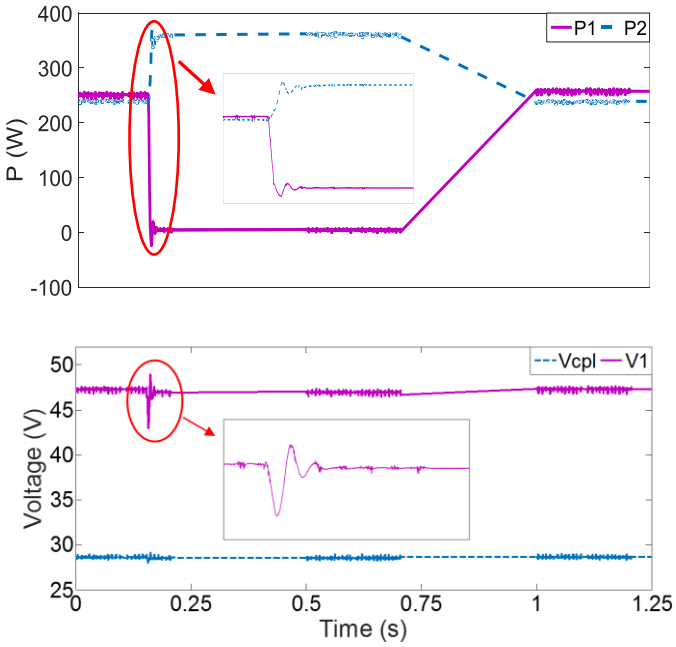

Fig. 1.9 Case 3: Proposed controller performance during interruption of a DER generation

Case 4- Cloud effect: In this simulation scenario, the PV unit connected to bus 2, experiences a generation reduction due to passing a moving object over the PV panels. This reduction will be for 0.2 second from t=0.9s to t=1.1s when 45% of the series modules are covered. The DER's controllers are able to keep the voltage stable on the nominal voltage. For instance, the voltage at bus 3 remains around 48V during the generation reduction of DER at bus 3, while the other resources compensate the power loss as shown Fig. 1.10. Although the PI controllers are also able to maintain the grid voltage, the output waveforms contain more noise and ripple that can be harmful for sensitive loads in the grid.

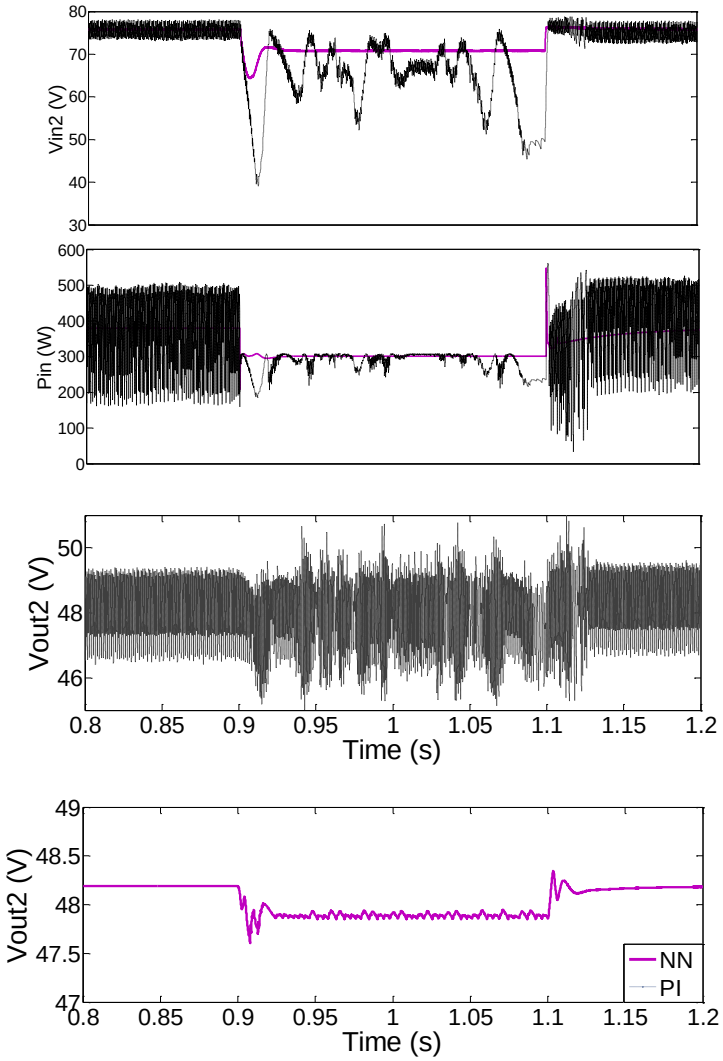

Fig. 1.10 Case 4: Proposed controller's performance in the presence of intermittent solar power

Case 5- Cloud effect: In this case hardware experimental study is conducted to observe cloud effects where the DER power generation at bus 2 is reduced due to passing cloud over the panels. The cloud effect is imitated by blocking the sunrays from reaching the panels using a large object. The employed measured signal in the control method is the output voltage. The other sources compensate this power loss and the grid voltage is stabilized around the nominal value as depicted in Fig. 1.11.

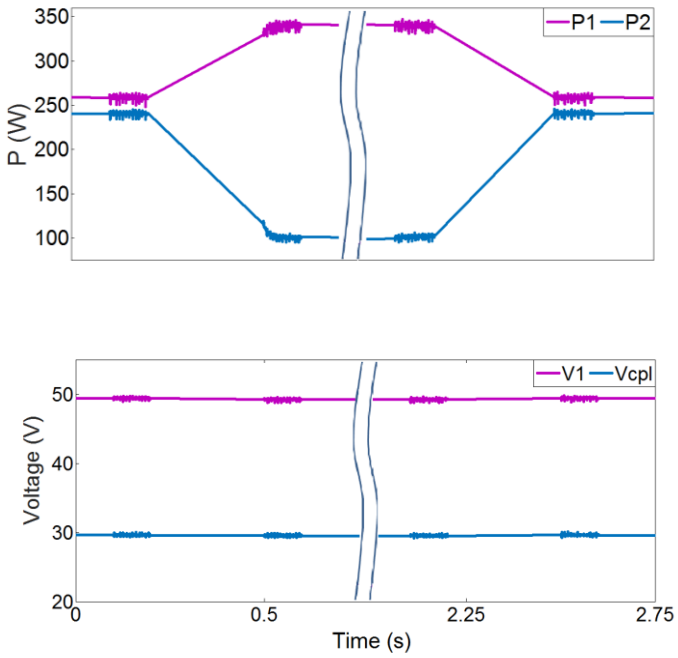

Fig. 1.11 Case 5: Proposed controller performance with generation changes due to cloud

Case 6- Input voltage control (measurement redundancy): In this hardware experimental study, performance of the controller is evaluated when the measured/controlled signal is the input voltage at D ER converter of bus 2. It is aimed to keep the output voltage around the nominal value by controlling the input voltage around the initial set value while disturbances take place in the system. Stabilizing the input voltage is expected to result in the stability of the other states. In this case, a large load (2kW at bus 10) is added to the grid and removed after 0.2 seconds. The controller is left unchanged from the previous case and only the measurement is switched to input voltage along with its corresponding set point. While the output voltage returns to the nominal value after the disturbance has been removed, the input voltage is stabilized at another operating point as shown in Fig 1.12. According to the presented decentralized control scheme in Section 4, the states are only bounded with finite steady-state error and asymptotic stability cannot be guaranteed. Thus, input voltage may stay stable with an error. However, this

does not affect the output voltage due to the power balance that is enforced by the controller. The slight reduction in the input voltage leads to an increased share of power for the connected DER. Thus, other DER will reduce power to ensure power balance in the dc circuit.

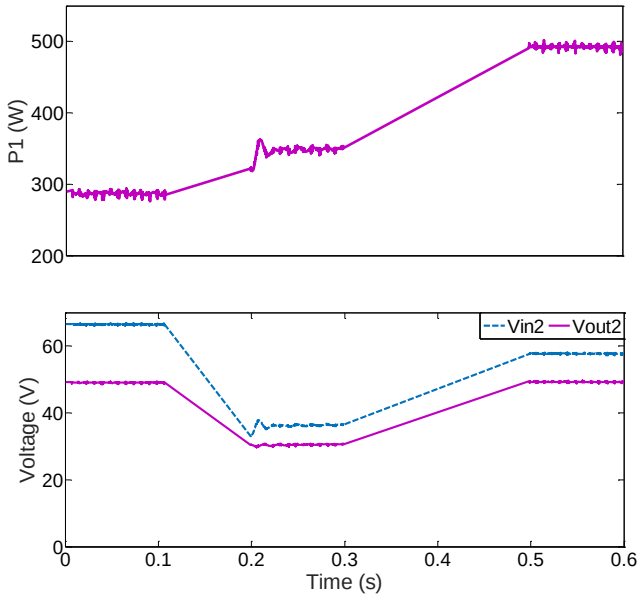

Fig. 1.12 Case 6: Proposed controller's performance with control on v_{in}

Case 7- Faulted circuit via voltage/current measurement (measurement redundancy): In this hardware experiment, robustness of the control scheme is evaluated in the fault conditions using hardware experiment. A low impedance fault (R_{fault}=1Ω at bus 11) is applied to the grid for 0.35 seconds. After voltage and power distortions due to the fault occurrence, the adaptive output-feedback controllers can attain the system stability using only the output voltage as depicted in Fig. 1.13. The output voltage and power of the DER at bus 1 as well as the CPL output voltage are shown, which confirm satisfying performance of the proposed method in the fault condition. Conversely, the PI controllers are not able to recover the voltage after the fault as depicted in Fig. 1.14.

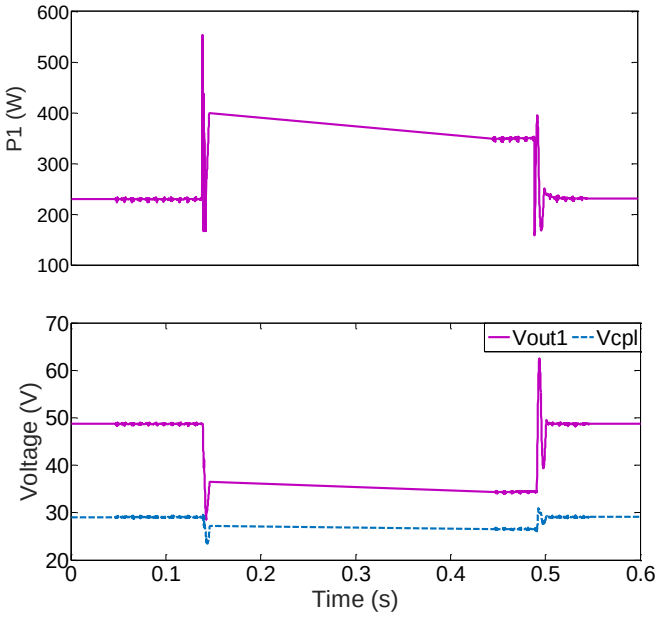

Fig. 1.13 Case 7: Proposed controller performance during a fault at bus 11 and control on v_{out}

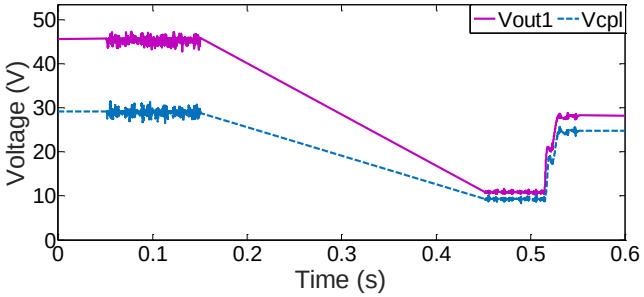

Fig. 1.14 Case 7: PI controller performance with fault at bus 11

Next, the same ground fault has occurred (at bus 11 for 0.35s) where the inductor current $i_{L,1}$ is employed as the measured/controlled variable at DER converter of bus 1 and the other converters utilize v_{out} as the controlled variable. The controller aims at keeping the current at the initial set value. The controller is left unchanged in case 7 and only the measurement is switched to inductor current along with its corresponding set point. After fault removal the proposed decentralized control scheme adjust the current at its initial value leading to the other states return to their initial points and the entire system stability as depicted in Fig. 1.15. Thus, the

approach is able to assure stability for the system using various measured states while current control approach can provide better performance in the fault conditions over the voltage since it prevents high amount of currents in the fault condition. The grid and CPL voltage achieve their nominal values after the fault removal and system stability is attained via current control as depicted.

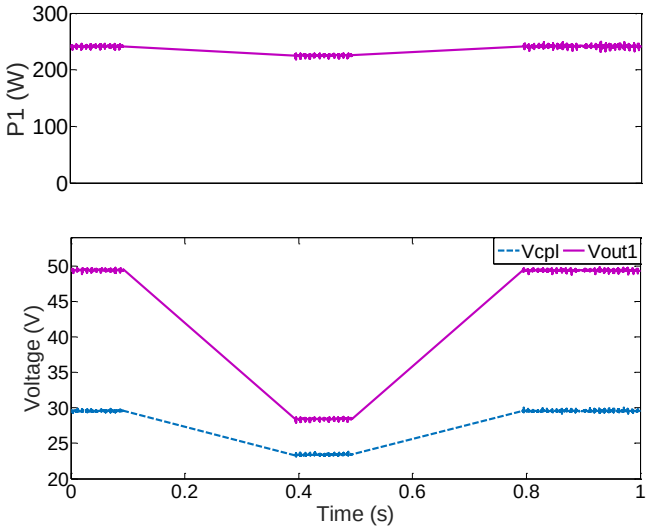

Fig. 1.15 Case 7: Proposed controller's performance in fault condition with control on i_L.

1.6 Conclusion

In this work, a decentralized discrete-time model for the interconnected dc grid is developed. The dc system consists of resistive loads as well as constant power loads and the photovoltaic sources that are coupled to the dc network via dc-dc buck converters. Decentralized adaptive output-feedback neural network controllers are proposed to guarantee the entire system stability and address the destabilizing effect of the CPLs, as a crucial issue in the dc systems. The proposed controller utilize only one measured state of the local converter and the other unknown states and interconnection dynamics are approximated through active learning property of the neural network to stabilize the entire system using the decentralized approach. In addition, the

proposed method provides measurement redundancy that is use of any other measured signals such as voltages or currents, in case of loss of main signal to increase system reliability. Simulation and experiment results are presented to validate system efficiency and it is shown that the proposed controller can noticeably diminish the voltage and power variation triggered by faults and disturbances and maintain system stability.

1.7 References

[1] T. Dragicevic, X. Lu, J. C.Vasquez, and J.M.Guerrero, "DC microgrids-Part I: A review of control strategies and stabilization techniques," IEEE Trans. Power Electron., vol. 31, no. 7, pp. 4876–4891, Jul. 2016.

[2] T.Dragicevic, X. Lu, J. C.Vasquez, and J.M.Guerrero, "DC microgrids— Part II: A review of power architectures, applications and standardization issues," IEEE Trans. Power Electron., vol. 31, no. 5, pp. 3528–3549, May 2016.

[3] J. M. Guerrero, J. C. Vasquez, J. Matas, L. G. de Vincu˜na, and M. Castilla, "Hierarchical control of droop-controlled ac and dcmicrogrids –Ageneral approach toward standardizationn," IEEE Trans. Ind. Electron., vol. 58, no. 1, pp. 158–172, Jan. 2011.

[4] C. Jin, P. Wang, J. Xiao, Y. Tang, and F. H. Choo, "Implementation of hierarchical control in dc microgrids," IEEE Trans. Ind. Electron., vol. 61, no. 8, pp. 4032–4042, Aug. 2014.

[5] D. Chen and L. Xu, "Autonomous dc voltage control of a dc microgrid with multiple slack terminals," IEEE Trans. Power Syst., vol. 27, no. 4, pp. 1897–1905, Nov. 2012.

[6] L. Ding, Z. Ma, P. Wall, and V. Terzija, "Graph Spectra Based Controlled Islanding for Low Inertia Power Systems" IEEE Trans. Power Delivery, vol. 32, no. 1, pp. 302-309, Feb. 2017.

[7] E. Rakhshani, and P. Rodriguez, "Inertia Emulation in AC/DC Interconnected Power Systems Using Derivative Technique Considering Frequency Measurement Effects" IEEE Trans. Power Systems, vol. 32, no. 5, pp. 3338-3351, Sep. 2017.

[8] A. Kwasinski and C. N. Onwuchekwa, "Dynamic behavior and stabilization of dc microgrids with instantaneous constant-power loads," IEEE Trans. Power Electron., vol. 26, no. 3, pp. 822–834, Mar. 2011.

[9] P.W. Sauer and M. A. Pai, “Power system dynamics and stability,” Stipess, Jan. 2007

[10] A. Moayedi and A. Davoudi, “Unifying distributed dynamic optimization and control of islanded microgrid,” IEEE Trans. Power Electron., vol. 32, no. 3, pp. 2329–2346, Mar. 2017.

[11] S. Augustine, L. Lakshminarasamma and M. Mishra, “Control of photovoltaic-based low-voltage dc microgrid system for power sharing with modified droop algorithm,” IET. Power Electron., vol. 9, no. 6, pp. 1132–1143, Nov. 2015.

[12] A. Khorsandi, M. Ashourloo, H. Mokhtari and R. Iravani, “Automotic droop control for a low voltage dc microgrid,” IET. Gener. Transm. Distrib, vol. 10, no. 1, pp. 41–47, Jul. 2015.

[13] A. Khorsandi, M. Ashourloo, and H. Mokhtari, “A decentralized control method for a low-voltage DC microgrid,” IEEE Trans. Energy Conversion., vol. 29, no. 4, pp. 793–801, Dec. 2014.

[14] B. Berggren, K. Lindén, and R. Majumder, “DC Grid Control Through the Pilot Voltage Droop Concept—Methodology for Establishing Droop Constants” IEEE Trans. Power Systems, vol. 30, no. 5, pp. 2312-2320, Sep. 2015.

[15] K. Rouzbehi, A. Miranian, J. I. Candela, A. Luna, and P. Rodriguez, “A Generalized Voltage Droop Strategy for Control of Multiterminal DC Grids” IEEE Trans. Industry Applications, vol. 51, no. 1, pp. 607-618, Jan. 2015.

[16] M. D. Cook, G. G. Parker, R. D. Robinett, and W. W. Weaver, “Decentralized Mode-Adaptive Guidance and Control for DC Microgrid” IEEE Trans. Power Delivery, vol. 32, no. 1, pp. 263-271, Feb. 2017.

[17] J. Hu, J. Duan, H. Ma, and M. Chow, “Distributed Adaptive Droop Control for Optimal Power Dispatch in DC Microgrid” IEEE Trans. Industrial Electronics, vol. 65, no. 1, pp. 778-789, Jan. 2018.

[18] P. Prabhakaran, Y. Goyal, and V. Agarwal, “Novel Nonlinear Droop Control Techniques to Overcome the Load Sharing and Voltage Regulation Issues in DC Microgrid” IEEE Trans. Power Electronics, vol. 33, no. 5, pp. 4477-4487, May 2018.

[19] A. Emadi, A. Khaligh, C. H. Rivetta, and G. A. Williamson, “Constant power loads and negative impedance instability in automotive systems: Definition, modeling, stability, and

control of power electronic converters and motor drives," IEEE Trans. Vehic Tech., vol. 55, no. 4, pp. 1112–1125, 2006.

[20] P. Liutanakul, A. Awan, S. Pierfederici, B. Nahid-Mobarakeh, and F. Meibody-Tabar, "Linear stabilization of a dc bus supplying a constant power load: A general design approach," IEEE Trans. Power Electronics, vol. 25, no. 2, pp. 475–488, 2010.

[21] A. M. Rahimi and A. Emadi, "Active damping in dc/dc power electronic converters: A novel method to overcome the problems of constant power loads," IEEE Trans. Indust Elect, vol. 56, no. 5, pp. 1428–1439, 2009.

[22] X.Liu, A.J. Forsyth, and A.M.Cross, "Negative input-resistance compensator for a constant power load," IEEE Trans. Industrial Electronics, vol. 54, no. 6, pp. 3188–3196, 2007.

[23] A. M. Rahimi, G. A. Williamson, and A. Emadi, "Loop-cancellation technique: A novel nonlinear feedback to overcome the destabilizing effect of constant-power loads," IEEE Tran Veh. Tec., vol.59, no.2, pp. 650–661, 2010.

[24] C. N. Onwuchekwa and A. Kwasinski, "Analysis of boundary control for buck converters with instantaneous constant-power loads," IEEE Trans. Power Electronics, vol. 25, no. 8, pp. 2018–2032, 2010.

[25] P. Magne, B. Nahid-Mobarakeh, and S. Pierfederci, "Large-signal stabilization of a dc-link supplying a constant power load using a virtual capacitor: impact on the domain of attraction," IEEE Trans. Industrial Applications, vol. 48, no. 3, pp. 878–887, 2012.

[26] D. Marx, P. Magne, B. Nahid-Mobarakeh, S. Pierfederci, and B. Davat, "Large signal stability analysis tools in dc power systems with constant power loads and variable power loads-a review," IEEE Trans. Power Electronics, vol. 27, no. 4, pp. 1773–1787, 2012.

[27] C. Rivetta and G. A. Williamson, "Large-signal analysis and control of buck converters loaded by dc–dc converters," in Proc. IEEE Power Electron. Spec. Conf., Aachen, Germany, June 2004, vol. 5, pp. 3675–3680.

[28] M. Cupelli, M. Mirz, and M. P. Carro, "Hardware in the loop implementation of a disturbance based control in MVDC grids," Proc. of Power & Energy Society General Meeting, July 2015.

[29] M. Cupelli, M. Mirz, and A. Monti, "Application of backstepping to MVDC ship power systems with constant power loads," Proc. of Electrical Systems for Aircraft, Railway, Ship Propulsion and Road Vehicles (ESARS), March 2015.

[30] G. Sulligoi, D. Bosich, G. Giadrossi, et al., and A. Monti, "Multiconverter Medium Voltage DC Power Systems on Ships: Constant-Power Loads Instability Solution Using Linearization via State Feedback Control," IEEE Trans. Smart Grid., vol. 5, no. 5, pp. 2543–2552, Sep. 2014.

[31] G. Sulligoi, D. Bosich, L. Zhu, M. Cupelli and A. Monti, "Linearizing Control of Shipboard Multi-Machine MVDC Power Systems feeding Constant Power Loads," Proc. of 2012 IEEE Energy Conversion Congress and Exposition (ECCE), Sep. 2012.

[32] L. Shen, D. D. Lu, Y. Wang, "Geometric maximum power point tracking and sliding mode control of a bidirectional grid connected single phase two-stage photovoltaic system with DC loads" IET Renew. Power Gener., vol. 10, no. 9, pp. 1310-1317, Jun. 2016.

[33] M. Su, Z. Liu, Y. Sun, H. Han, and X. Hou, "Stability Analysis and Stabilization Methods of DC Microgrid With Multiple Parallel-Connected DC–DC Converters Loaded by CPLs" IEEE Trans. Smart Grid, vol. 9, no. 1, pp. 132-142, Jan. 2018.

[34] J. Wang, C. Zhang, S. Li, J. Yang, and Q. Li, "Finite-Time Output Feedback Control for PWM-Based DC–DC Buck Power Converters of Current Sensorless Mode" IEEE Tran. Control Systems Technology, vol. 25, no. 4, pp. 1359-1371, Jul. 2017.

[35] V. Calderaro, G. Conio, V. Galdi, et al. , "Opti- mal decentralized voltage control for distribution systems with inverter- based distributed generators," IEEE Trans. Power Syst., vol. 29, no. 1, pp. 230–241, Jan. 2014.

[36] S. Kazemlou and S. Mehraeen, "Novel decentralized control of power systems with penetration of renewable energy sources in small-scale power systems," IEEE Trans. Energy Conv, vol. 29, no. 4, pp. 851–861, Dec. 2014.

[37] V. Nasirian, S. Moayedi, A. Davoudi, and F. L. Lewis, "Distributed cooperative control of dc microgrids," IEEE Transactions on Power Electron., vol. 30, no. 4, pp. 2288-2303, April 2015.

[38] E. Gyurkovics and T. Takacs, "Stabilization of discrete-time interconnected systems under control constraints," IEE Proceedings-Control Theory and Applications, vol. 147, no. 2, pp. 137–144, 2000.

[39] Y. H. Lin and K. S. Narendra, "A new error model for adaptive systems," IEEE Trans. Automatic Control, vol. 25, no. 3, pp. 585–587, 1980.

[40] S. Jain and F. Khorrami, "Decentralized adaptive control of a class of large-scale interconnected nonlinear systems," IEEE Trans. Automatic Control, vol. 42, no. 2, pp. 136–154, 1997.

[41] J.T. Spooner and K.M. Passino, "Adaptive control of a class of decentralized nonlinear systems," IEEE Trans. Automatic Control, vol. 4 , no. 2, pp.280–284, 1996.

[42] S. Mehraeen, S. Jagannathan, and M. L. Crow, "Decentralized adaptive neural network state and output feedback control of a class of interconnected nonlinear discrete-time systems," Proc. of American Control Conference (ACC), Montreal, Canada, June 2012, pp. 6406–6411.

[43] S. Kazemlou and S. Mehraeen, "Decentralized discrete-time adaptive neural network control of interconnected dc distribution system," IEEE Trans. Smart Grid, vol.5, no.5, pp. 2496–2507, Sep. 2014.

[44] S. Kazemlou, S. Mehraeen, H. Saberi, and S. Jagannathan, "Stability of the Small-Scale Interconnected DC Grids via Output-Feedback Control" IEEE Journal of Emerging and Selected Topics in Power Electronics, vol. 5, no. 3, pp. 960-970, Sep. 2017.

[45] S. Mehraeen, S. Jagannathan, and M. L. Crow, "Power System Stabilization Using Adaptive Neural Network-Based Dynamic Surface Control" IEEE Trans. Power Syst., vol. 26, no. 2, pp. 669-680, May. 2011.

[46] M. Chen, and S. S. Ge, "Adaptive Neural Output Feedback Control of Uncertain Nonlinear Systems With Unknown Hysteresis Using Disturbance Observer" IEEE Trans. on Industrial Electronics, vol. 62, no. 12, pp. 7706-7716, Dec. 2015.

[47] L. Long, and J. Zhao, "Decentralized Adaptive Neural Output-Feedback DSC for Switched Large-Scale Nonlinear Systems" IEEE Trans. Cybernetics, vol. 47, no. 4, pp. 908-919, Apr. 2017.

[48] Olivares, D. E., Mehrizi-Sani, A., Etemadi, A. H., et al., "Trends in microgrids," IEEE Trans. Smart Grid, vol. 5, no. 4, pp. 1905–1919, Jul. 2014.

[49] N. Mohan, T. M. Undeland, and W. P. Robbins, "Power Electronics: Converters, Applications, and Design" Hoboken, NJ, USA: Wiley, 2002.

[50] C. T. Chen, Linear System Theory and Design. Oxford Uinv. Press, Nov. 2012.

[51] F. L. Lewis, S. Jagannathan, and A. Yesildirak, Neural Network Control of Robot Manipulators and Non-Linear Systems. New York, NY, USA: Taylor & Francis, 1998.

[52] S. Mehraeen and S. Jagannathan, "Decentralized adaptive neural network state and output feedback control of a class of interconnected nonlinear discrete-time systems," in Proc. Amer. Control Conf. (ACC), Montreal, QC, Canada, Jun. 2012, pp. 6406–6411.

[53] B. Igelnik, and Y. Pao, "Stochastic choice of basis functions in adaptive function approximation and the functional-link net" IEEE Trans. Neural Networks, vol. 6, no. 6, p

CHAPTER 2
A SIMULTANEOUS VOLTAGE AND PHASE CONTROL SCHEME FOR PHOTOVOLTAIC DISTRIBUTED GENERATION UNITS IN SMALL-SCALE POWER SYSTEMS

2.1 Introduction

Renewable energy resources have recently attracted more attention as clean and abundant sources of energy [1-5]. Harvesting energy from distributed energy resources (DERs) such as solar, wind, wave, and the tidal power are becoming more efficient and practical. Mature technologies for installing distributed generation (DG) units become more available and cost effective. This results in an increased demand for distributed generation installations that exploit renewable power; especially, solar and wind power whose considerable share of the total consumed energy is imminent.

The solar power is probably the most available renewable energy in residential and commercial scales. Power electronic converters are used to interface the photovoltaic (PV) units to the ac gird through dc-dc and dc-ac power electronic converters. It has been a common strategy for PV systems to be controlled such that the maximum available energy is extracted from the solar panels. For this purpose, the inverter is controlled as a current-source inverter (CSI) to inject the maximum current to the grid [6]. However, in a grid that the DGs generate a considerable share of energy, this strategy will not be efficient. In such a grid, DGs should contribute in voltage and frequency regulation, system stability, and all other issues that arise in a conventional power system similar to the synchronous generators. In the conventional power systems, synchronous machines are the main sources of electric power. During the past decades, this basic part of the system is well studied and analysed by researchers and engineers. Several control schemes are designed for the synchronous machines including voltage, frequency, active,

and reactive power controls. Due to the existence of such mature technologies, it is rational to utilize them in the inverter-base solar power generation. Voltage source inverters (VSIs) are then required to make possible the implementation of the mentioned control mechanisms [7, 8].

The modelling, control, and stability of the parallel VSIs in a microgrid is investigated in [9]. The control mechanism consists of two levels: a) a primary control with current and voltage loops that is a droop-based control, and b) a secondary control that is a local centralized control for power sharing and restoring the voltage magnitude and mitigate frequency mismatch resulted from the primary control. Also, a droop-based control is presented in [10], where the system's parameters are estimated first and then, active and reactive powers are delivered to the grid independently. However, these works consider a constant-voltage dc link, an assumption that may not be feasible in larger PV units. Note that, capacitors are more suitable in the dc link when power fluctuations (a factor that reduces the battery's lifetime) are significant. Droop-based strategies are proposed for ac and dc sub grids and the interlinking converter in a hybrid system as well as other inverter-based DGs to control the active and reactive powers and mitigate the frequency and voltage fluctuations with time constants of several seconds in the secondary control loops [11, 12].

Recently, several algorithms have been proposed to control the inverters similar to synchronous generators for more rapid response to stability concerns. The concept of "Synchronverter" first proposed in [13], is an inverter that is controlled to operate like a synchronous generator for frequency and voltage control. While the active and reactive power control are doable similar to that in the synchronous machine, in most of these works the dc link is connected to a battery that provides a constant dc-link voltage, and thus, no voltage

fluctuations are present in the dc link under active and reactive power disturbances. By contrast, the photovoltaic generation units connected to the dc-link capacitors are prone to significant dc-link voltage variations in the absence of an appropriate voltage control scheme.

So far, all the above mentioned approaches assume a constant voltage at the dc link. Installing a battery bank at the dc link can result in a constant voltage; however, imposing fast transients to the batteries degrades them and reduces their lifetime significantly [14]. A capacitor should be installed at the dc link to respond to the fast transients such that the battery can be used for longer term applications such as load shaping, peak shaving, etc.

Smart inverters are recently proposed to add reactive power control to the conventional inverter-based photovoltaic units in order to maintain a satisfactory voltage level. In [15] a volt/Var control of PV inverters is presented for various irradiance and voltages at the Point of Common Connection (PCC). The controller modifies the solar unit reactive power according to the voltage sensitivity indices to maintain the voltage. In [16], a distributed mechanism based on the conventional Volt/Var droop control functions is applied to the PV inverters and the stability of the controller is investigated. These strategies can support the reactive power to maintain the voltage within the permissible margins and mitigate the voltage fluctuations. However, the photovoltaic units are not characterized and modelled in the controller development, and thus, the dc-link voltage variations are not discussed.

In contrast, a detailed model of the photovoltaic generation units is described in this paper where the dc-link voltage stability is explicitly considered and simultaneous output voltage and frequency control are targeted. A dc-dc buck converter is used to connect the photovoltaic unit to the inverter. The dc-link voltage is maintained via a capacitor that provides stored energy

and contributes to the system stability in transients, similar to the synchronous generator rotating mass. An excitation-like mechanism is employed to control the inverter ac voltage through the inverter's amplitude modulation factor. Then, a fast droop controller varies the dc-dc converter's duty cycle to control the power balance at the capacitor terminals via photovoltaic output power. Once the capacitor voltage is controlled, the voltage angle at the inverter terminal, which is coupled with the capacitor voltage variations, is stabilized, and frequency stability is achieved as well [17, 18].

The rest of the paper is organized a follows: the proposed modelling and control scheme are presented in Section 2. Section 3 provides stability analysis of the interconnected grid. Simulation scenarios and results are given in Section 4. Finally, the conclusion remarks will be presented in Section 5.

2.2 System Topology and Proposed Control Scheme

A. System topology

The buck topology is used as the dc-dc converter of the proposed system. Although the boost converter poses higher output voltage, due to the stability problems, the buck converter is more reliable for the PV system [19, 20]. For increasing the voltage level, transformers at the ac side or topologies like forward converters that employ transformers for stepping up the voltage can be used, without affecting stability of the system [21]. There are two capacitors at the input and output of the dc-dc converter. The input capacitor provides a smoother voltage at the input, and the output capacitor, as will be discussed later, plays an important role in system stability.

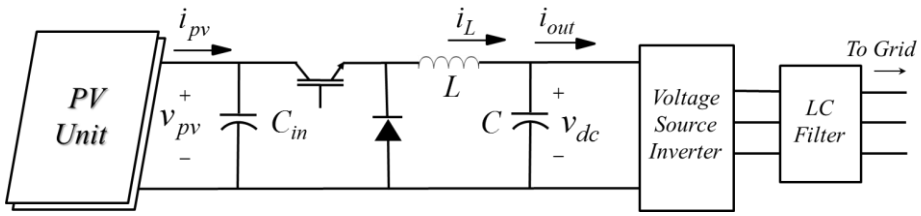

Fig 2.1. The entire system block diagram.

The primary source of energy is a PV unit. In order to realize a stable operation for the system, voltage of the PV should vary between the open circuit voltage (V_{oc}) and voltage at the maximum power point (V_{mpp}). The dc-dc converter duty ratio varies according to the ac side voltage and the modulation factor, to keep the PV's voltage in the permissible range. The dc-ac conversion is carried out using a three-phase two-level PWM inverter. The inverter is connected to the Point of Common Connection (PCC) through an LC filter and step up transformers. The entire system block diagram is depicted in Fig. 2.1.

B. Control Scheme

The dc-dc converter is connected to the inverter through the dc link capacitor. The energy stored in this capacitor acts like the kinetic energy stored in rotating mass of the synchronous generator. The size of the capacitor determines the amount of stored energy that is available at the dc link. However, higher size of the capacitor results in higher cost for the system. The amount of stored energy is also dependent on dc link voltage. Dynamic equations for the power at the dc link can be written as

$$CV_C\dot{V}_C = P_{in} - P_o \tag{1}$$

where P_{in} is the power that is injected to the capacitor from the dc-dc buck converter and comes from the primary source of energy that is a PV here, P_o is the delivered power to the inverter, and V_C is the capacitor voltage.

On the other hand, the inverter's delivered power to the grid can be written as

$$\overline{P}_e = BV_{inv}V\sin(\gamma - \theta) \tag{2}$$

where B is the admittance that connects the inverter to the grid, V_{inv} and γ are the voltage magnitude and phase angle at the inverter's output terminals, and V and θ are the grid bus voltage magnitude and phase angle. Neglecting the inverter's losses results in $\overline{P}_e = P_o$. In (2), B is constant, V and θ are also not under control and dictated by the grid, V_{inv} should also be within the allowable range (normally between 0.95 and 1.05pu). Then, the only variable that can be adjusted to control the inverter's output power is γ. A new variable λ is introduced to control γ in the inverter as

$$\lambda = \dot{\gamma} \tag{4}$$

Parameter λ resembles rotor speed (ω) in the synchronous generator. The rotor speed define the kinetic energy stored in the rotor as

$$\dot{\omega} = 1/M(P_m - P_{elec}) \tag{5}$$

where M is the inertia coefficient ($2H$ in seconds), P_m is the input mechanical power and P_{elec} is the output electrical power. In order to relate the new variable λ to the stored energy in the dc link capacitor, it can be defined as

$$\dot{\lambda} = (1/C)(P_{in} - P_o) \tag{6}$$

By using equation (1)

$$\dot{\lambda} = V_C \dot{V}_C \tag{7}$$

that yields

$$\lambda = (V_C{}^2 - V_{Co}{}^2)/2 \tag{8}$$

Hence, λ is the scaled changes in capacitor stored energy.

Equation (6) relates the output power at the ac side to the available power that comes from the primary source of energy at the dc side. In the synchronous generators, P_m is the input power that comes from the turbine and P_{elec} is the generator's output power that is delivered to the grid. Difference between input and output powers is the kinetic energy that is stored in the generator rotating mass and is a function of rotor speed and inertia coefficient. In the DG system, P_{in} is the input power that comes from the source of energy at dc side, P_o is the inverter's output power that is delivered to the power system. Difference between input and output powers is the stored energy at the dc-link capacitor that is a function of dc-link voltage and size of the capacitor.

In the synchronous generators, droop mechanism provides additional torque during disturbances in the power system. Any deviation from the synchronous speed causes an additional damping torque that opposes any change in the speed of the generator. Hence, the resultant torque helps maintain synchronism of the machine. This technology can be utilized to maintain the dc-link capacitor voltage. Thus, as an active power control strategy, any deviation from the steady state value of λ will result in some change in the dc-dc converter's duty cycle, D. This adjustment subsequently changes the operating point of the PV unit which alters its output power. Thus, any variation in λ follows by some change in the injected power which comes from

the dc side and helps maintain λ at its steady state value similar to operation of machine governor.

So far, the DG system is modeled and controlled to behave similar to classical model of a synchronous generator with a constant voltage source is behind the transient reactance. In order to provide voltage magnitude and consequently reactive power control, an excitation-like mechanism is employed. Similar to the rotor flux and field voltage in a synchronous generator, two new variables, E'_q and E_{fd}, are defined for the DG system. Thus, a new dynamic is added to the system as

$$\dot{E}'_q = \frac{1}{T_{d0}}\left(-(x_d/x'_d)E'_q + ((x_d - x'_d)/x'_d)V\cos(\gamma - \theta) + E_{fd}\right) \tag{9}$$

where x_{dr} , x'_{dr} are direct-axis synchronous and transient reactances, respectively, and T'_{d0} is direct-axis transient open-circuit time constant that can be selcted for the proposed model. Here, these parameters can be set as desired in contrast with the synchronous machines, where the parameters are constant for each machine. Thus, the excitation-like system is developed using preferred parameters. For instance, T'_{d0} that defines the excitation circuit time constant, can be set as preferred based on system requirements.

Then, E_{fd} is adjusted for voltage and reactive power regulation of the DG system. Varying E_{fd} alters E'_q as the rotor flux that in turn contributes to adjusting voltage magnitude of the synchronous machine. Taking into account (9) along with (4) and (6), the model resembles flux-decay model of the synchronous generator. The benefit of this model is to make possible application of all available technologies for a synchronous generator such as automatic voltage

regulator (AVR), power system stabilizer (PSS), etc. The output power of a synchronous generator that is described via flux-decay model is [22]

$$P_e = (1/x'_d)V[E'_q \sin(\gamma-\theta) - ((x_q - x'_d)/(2x_q))V\sin(2(\gamma-\theta))] \quad (10)$$

However, the inverter output power is as described in (1). In order to have an identical behaviour to the flux-decay model, inverter's output power should be equal to P_e in (10). By equating (10) and (2), V_{inv}, the voltage magnitude at the inverter's output terminals, is derived as

$$V_{inv} = \frac{E'_q \sin(\gamma-\theta) - \frac{x_q - x'_d}{2x_q} V\sin(2(\gamma-\theta))}{x'_d B\sin(\gamma-\theta)} \quad (11)$$

In order to attain this voltage, the inverter modulation factor, k_{inv}, is adjusted such that the fundamental harmonic of the voltage at inverter output terminal is V_{inv}.

Therefore, similar to the flux-decay model of a synchronous generator, according to (4), (6), and (9), the DG system is described via a third order dynamic equation where E'_q, γ, and λ are the state variables, and input power P_{in}, and field voltage, E_{fd}, are control inputs of the system. Figure 2.2 shows the relation between dc and ac dynamics and the active power control through the droop-like mechanism. Also, any change in the E_{fd} is reflected in V_{inv} and the inverter's modulation factor k_{inv}, as shown in (11). Thus, the excitation system controls the voltage amplitude using modulation factor, k_{inv}.

While the input power is controlled through the droop mechanism, the other input, E_{fd}, can be controlled via an AVR. The AVR receives the error between voltage set value and measured voltage magnitudes and generate the appropriate field voltage E_{fd} to attain the voltage at the set value. The voltage magnitude and reactive power regulation can be done through the AVR similar to the synchronous generator. However, using an AVR adds another dynamic to the

system wherein the field voltage E_{fd} will be the forth state variable and control inputs are voltage magnitude set value and input power. In addition, the PSS adds a modulation signal to the voltage controller input. Although more details can be taken into account; here, the focus is to propose the central framework of synchronous generator for DG units.

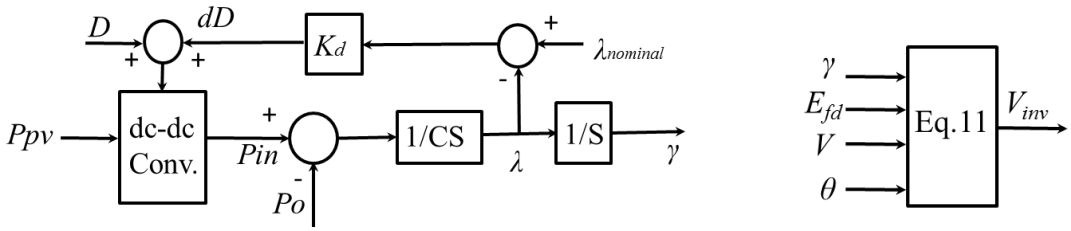

Fig 2.2. Voltage phase and magnitude control diagram

Remark 1: The modeling and control presented in this paper is a short-term analysis and must not be confused with the longer-term dynamics introduced by the maximum power point trackers (MPPTs) and daily load changes. Rather, the proposed approach studies disturbances that can cause rapid voltage fluctuations, which can adversely affect the PV power generation, and could potentially lead to the entire network instability. Thus, the slow dynamics of MPPT are ignored.

2.3 Simulation Results

Efficiency of the proposed scheme is investigated through simulations. The simulations are carried out using Matlab\Simulink. First, stable operation of the proposed method in stand-alone condition is evaluated in comparison to the Synchronverter model [13]. The parameters of the systems including the Synchronverter and the proposed model are listed in Table 2.1. In [23], it is shown that the stability of the Synchronverter is dependent to an external series resistance at the inverters terminals. Presence of this series resistance decrease the efficiency of

the Synchronverter, this deficiency is addressed by modifying the original Synchronverter model.

Case 1- Load change: As the first simulation scenario, the synchronverter and proposed scheme are applied to a stand-alone DG unit that is feeding a local load. At t=2s the load is stepped up from 200W to 250W for half a second and then returns to its initial value. Satisfying performance of the proposed control method is shown in Fig. 2.3. The voltage at the PV terminals decrease to provide more power at the output based on PV characteristics. Subsequently, the buck converter duty cycle is increased to push back the dc link voltage to the initial value. Stable dc link voltage results in steady operation of the entire DG unit. In addition, the field voltage (E_{fd}) is set on the nominal value to achieve nominal voltage value at the inverter output terminals. On the other hand, the Synchronverter cannot restore dc link voltage and failed to feed the load appropriately as demonstrated in Fig. 2.4. A PI controller is applied to adjust the dc link voltage at the initial value in the Synchronverter model.

Table 2.1. System parameters

Parameter	Value	Parameter	Value
- PV short circuit current	I_{sc} =9.71 A	x_d	0.2 pu
- PV open circuit voltage	V_{oc} =39.5 V	x'_d	0.06 pu
- PV maximum power	V_{oc} =280 W	x_q	0.19 pu
- Conv. capacitors	C_{in}=1000	T_{do}	7s
- Conv. Capacitor	C_{out}=1000 μF	B	5
- Conv. inductance	L=2.5 mH	D_p	0.2026
- Switching frequency	f_s=10 kHz	D_q	117.88
- Line resistances	R_{Line}= 0.5 Ohm	τ_f	0.002
- Line inductances	L_{Line}= 20 mH	τ_v	0.002
- V_{grid}	$V_{(L-L)}$=200		

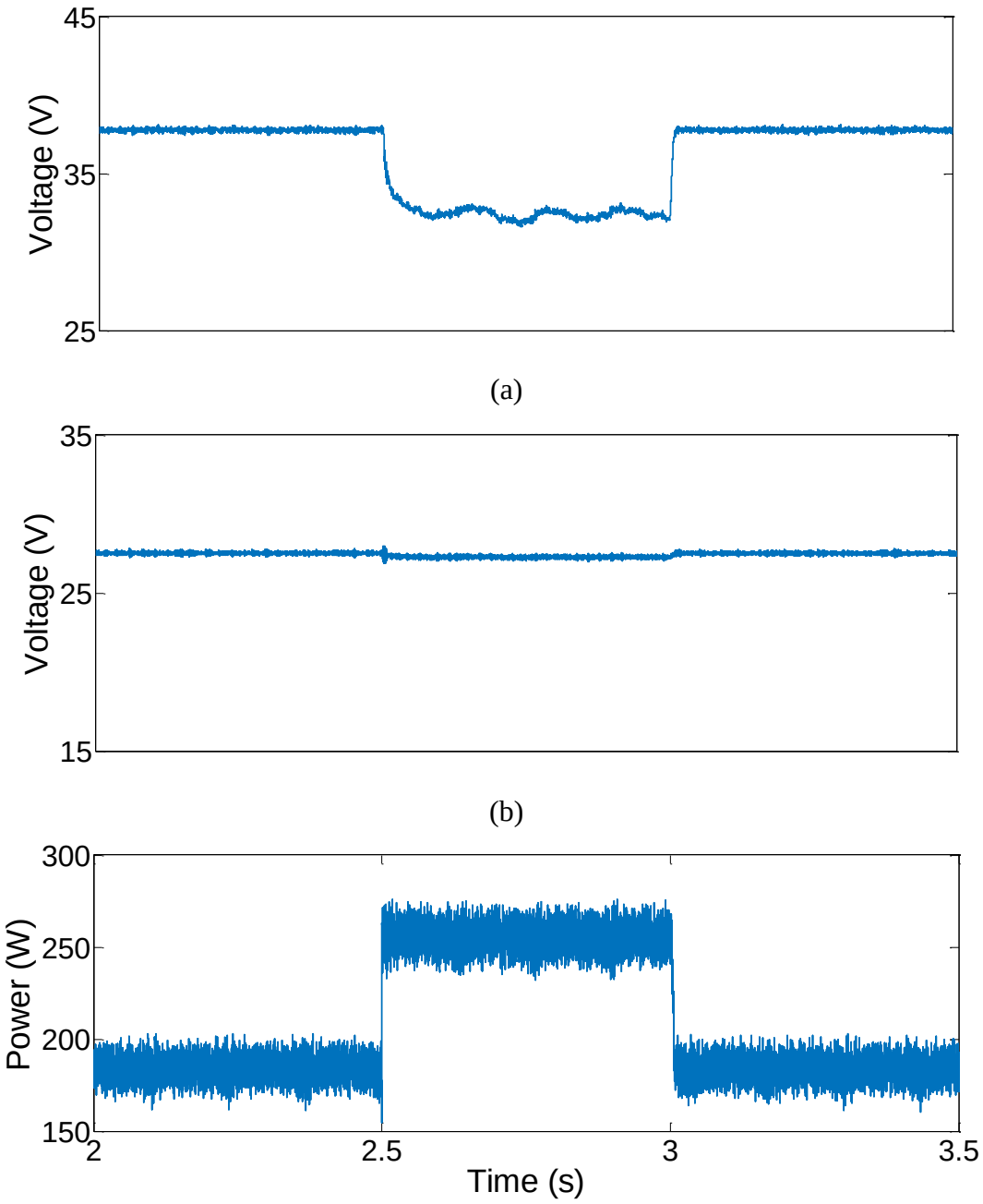

Fig 2.3. Case 1: The proposed model operation in stand-alone operation: a) Voltage at the PV terminals, b) Voltage at the DC link c) Output power

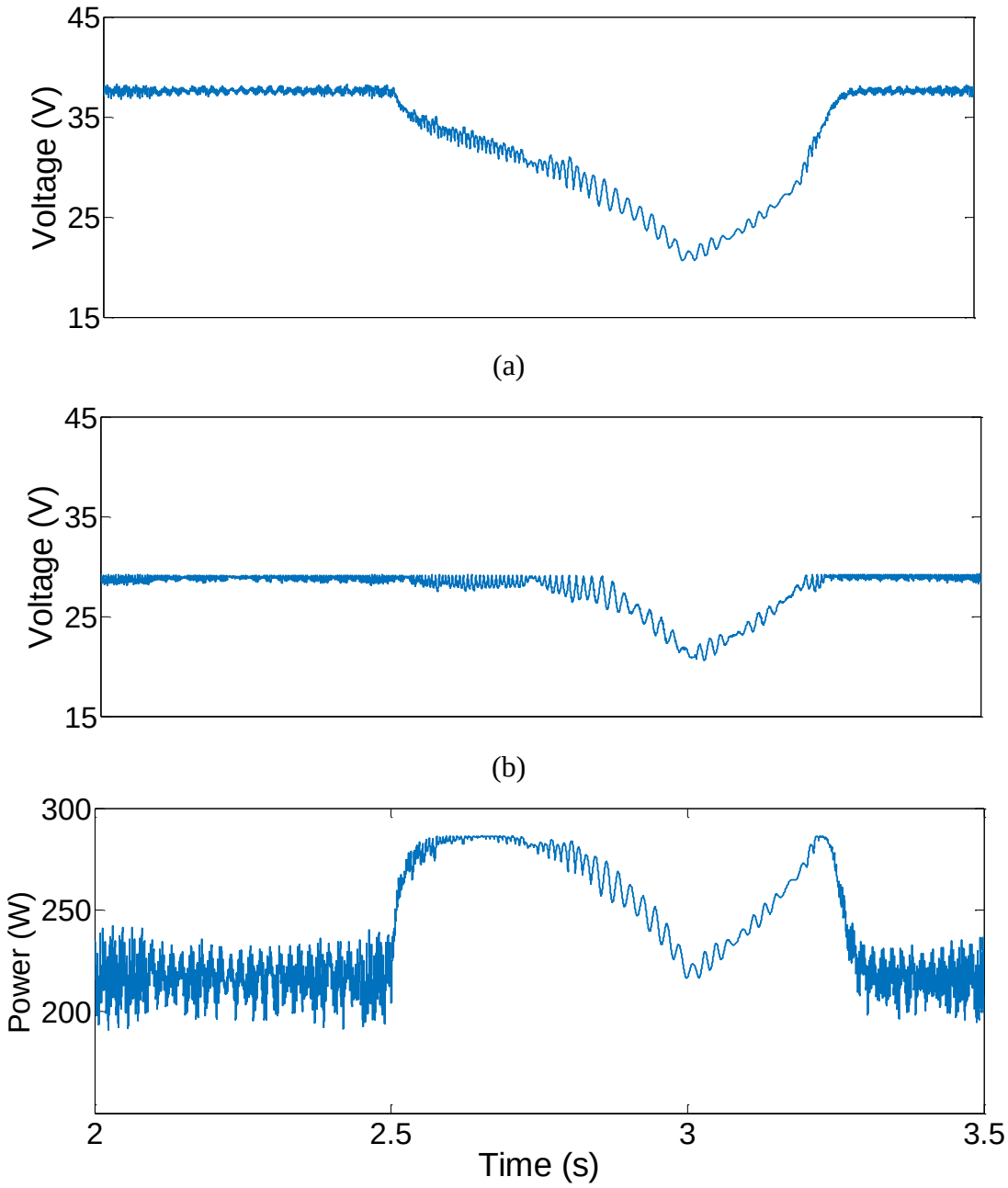

Fig. 2.4. Case 1: Synchronverter performance in stand-alone operation: a) Voltage at the PV terminals, b) Voltage at the DC link c) Output power

Case 2- Load change: In the second simulation scenario, efficiency of the control scheme is evaluated in the benchmark low voltage microgrid that is shown in Fig. 2.5. Two PV-based

DG units equipped with the proposed control system feed five resistive loads in the grid. DG 1 is composed of three PV panels in series and DG 2 include two panels in series. As the second simulation scenario, Load 4 is connected to the grid at t=1s and removed after half a second while DGs are feeding the grid under normal conditions. The control method is capable of sharing the load between the DGs and system sustain its stability after first swings. The voltage at the PV terminal decreases to extract more power out of the PV, then buck converter's duty cycle increases to maintain the dc link voltage at the initial value as shown in Fig. 2.6 and Fig. 2.7. In addition, the voltage magnitude is regulated through the inverter's modulation factor according to excitation-like mechanism in (11). The modulation factor (K_{inv}) varies to adjust the voltage magnitude at the nominal value as shown in Fig. 2.8. It should be mentioned that the E_{fd} remains constant; however, it is internal dynamics of the synchronous generator-like model that tends to keep the output voltage constant.

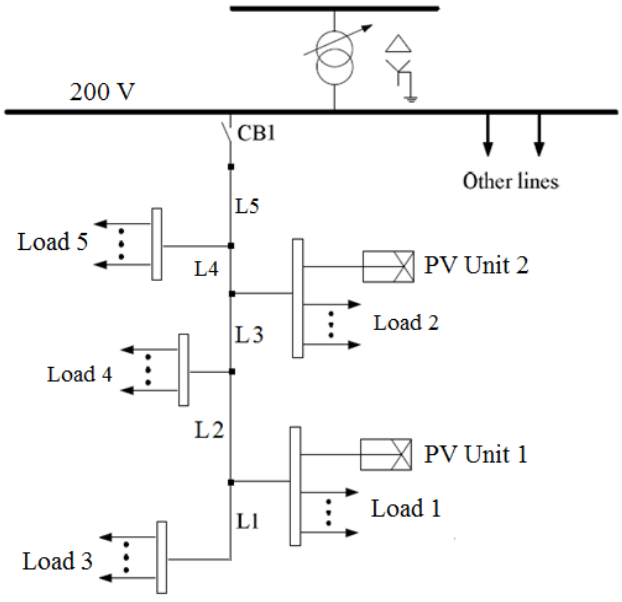

Fig. 2.5. Benchmark low voltage microgrid

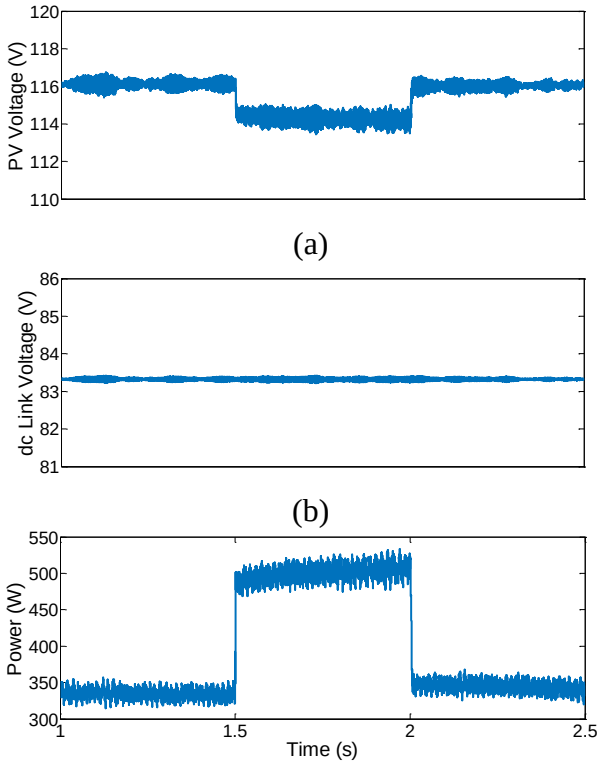

Fig. 2.6. Case 2: DG#1 performance during load change: a) PV output voltage, b) dc link voltage, and c) DG output power

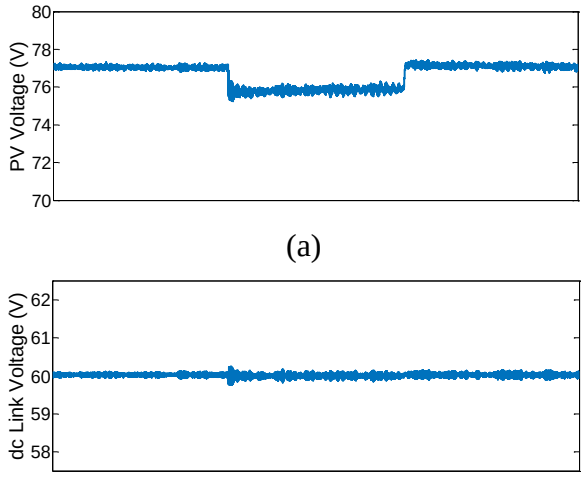

Fig. 2.7. Case 2: DG#2 performance during load change: a) PV output voltage, b) dc link voltage, and c) DG power

(Fig. 2.7 cont'd)

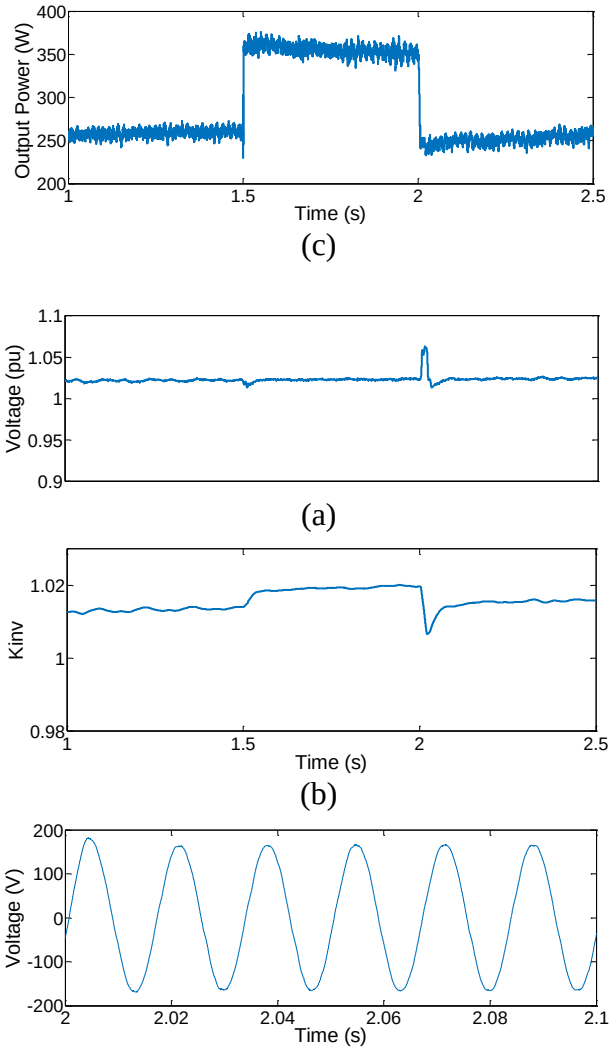

Fig. 2.8. Case 2: Voltage at DG#1: a) Output voltage RMS value, b) Inverter modulation factor, and c) Zoomed voltage waveform

Case 3- Cloud effect: As the third simulation scenario, cloud effect on PV-based DG units is investigated. In the third simulation scenario, DG units are feeding the grid in normal condition while a moving cloud passes over one of the DG's PV panels and decreases the generation capacity of the DG by 50% for half a second. Then, voltage over that PV panels decreases to extract more power out of the panels, dc-dc converter duty cycle is also increased to maintain the dc link voltage around initial set value. On the other hand, voltage over the other

DG's PV panels dropped to inject more power to the grid and compensate power loss of the other DG unit as shown in Fig. 2.9 and Fig. 2.10.

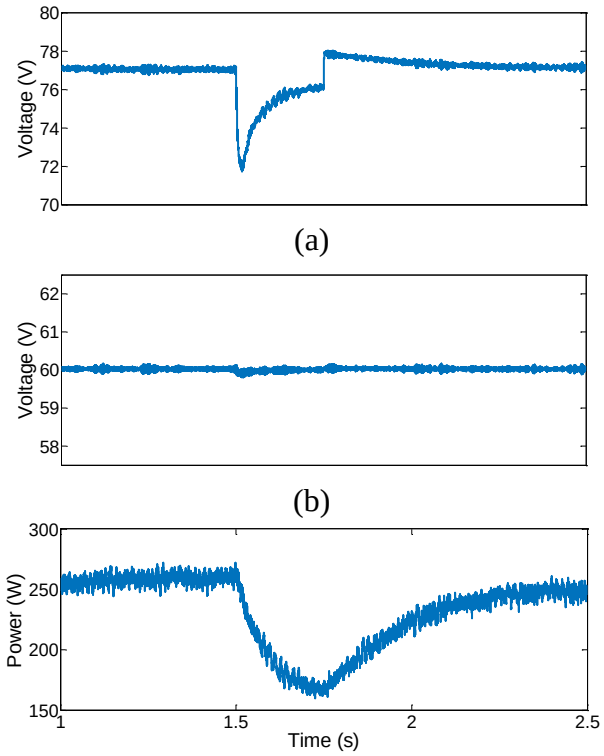

Fig. 2.9. Case 3: DG#1 performance in the cloud scenario: a) PV output voltage, b) dc link voltage, and c) DG output power

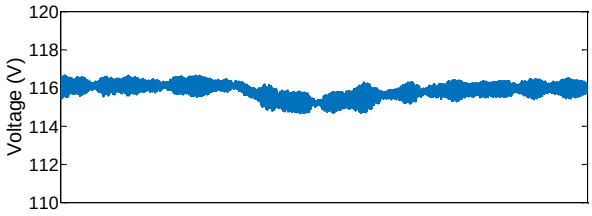

(a)

Fig. 2.10. Case 3: DG#2 performance in the cloud scenario: a) PV output voltage, b) dc link voltage, and c) DG output power

(Fig. 2.10 cont'd)

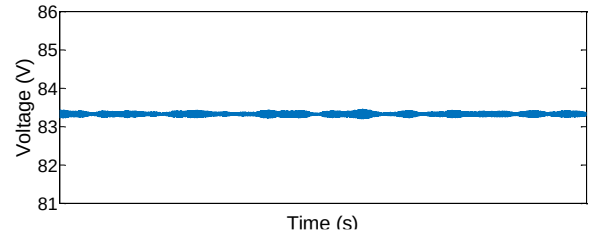

(b)

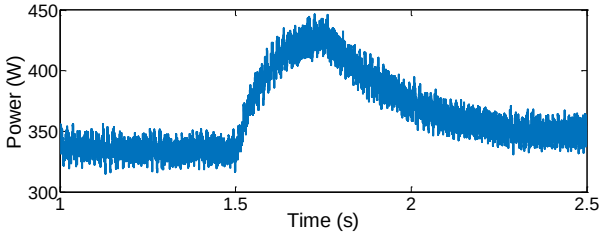

(c)

2.4 Experimental Results

An experimental setup is built to validate stable operation of the system and dynamic voltage control capability. The proposed control scheme is applied to the DG unit that is composed of a dc-dc buck converter and a dc-ac converter as depicted in Fig. 2.11. dSPACE Microlabbox control platform is used to apply the control method using MATLAB. The PV panels outputs are connected to dc-dc buck converters. The buck converter provides a stable dc voltage at the output. Subsequently, the inverter generate a three phase ac voltage using the stable dc voltage. In order to eliminate the harmonics and create a sinusoidal waveform out of the inverter output LC filters are employed. The resultant voltage feed a local load and also the grid through step up transformers that are arranged in Delta-Star configuration. The developed microgrid is based on benchmark low voltage microgrid in Fig. 2.5.

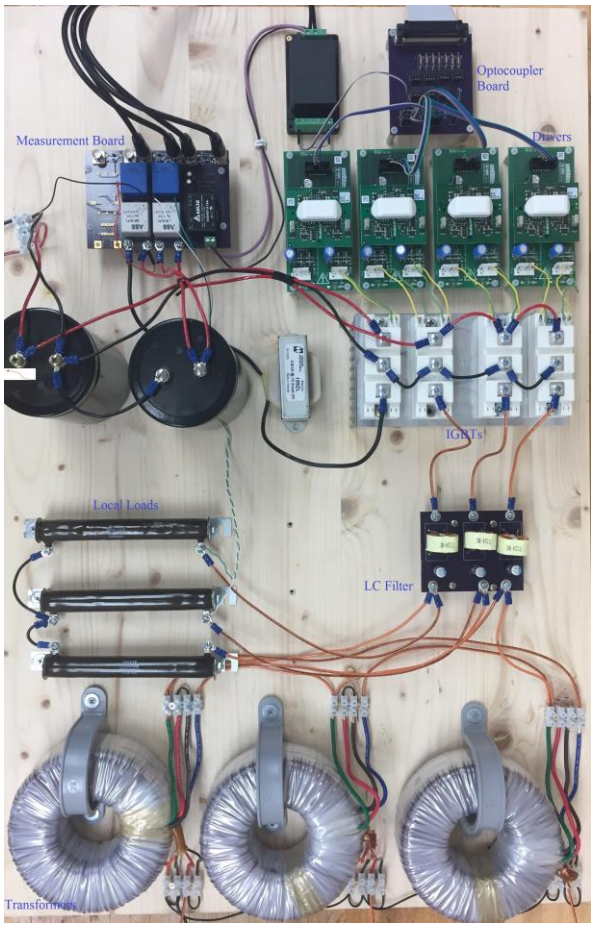

(a)

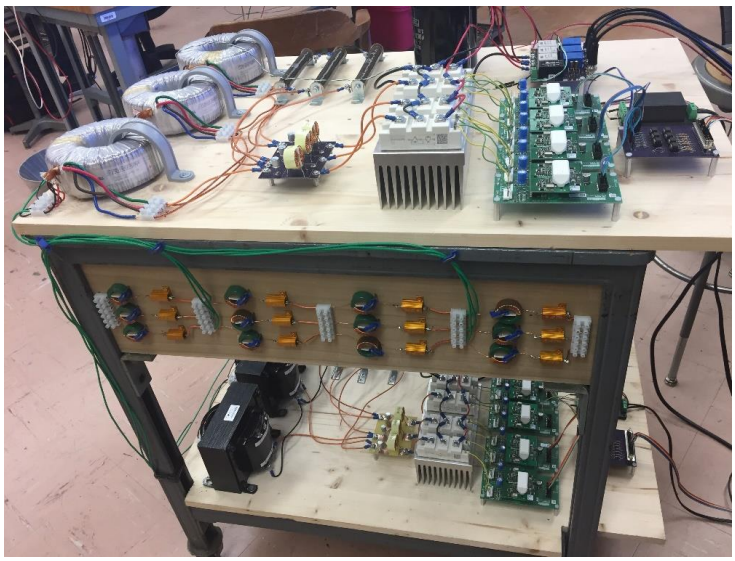

(b)

Fig 2.11. Experimental setup a) Detailed graph of a DG unit b) Implemented low voltage microgrid

Case 4- Load Change: In the first experiment scenario, two PV-based DG units are feeding the loads in the low voltage microgrid. At t=6.75s load 4 is added to the grid and removed after four seconds. Dc link voltage, dc-dc converter's inductor current, and output power of each DG is shown in Fig. 2.12 and Fig. 2.13. The presented results demonstrate desired performance of the entire system in sharing the added load properly between the sources while the dc links voltages remain stable around the initial values. Voltage of the grid is also shown in Fig. 2.14 that shows satisfactory condition of the grid.

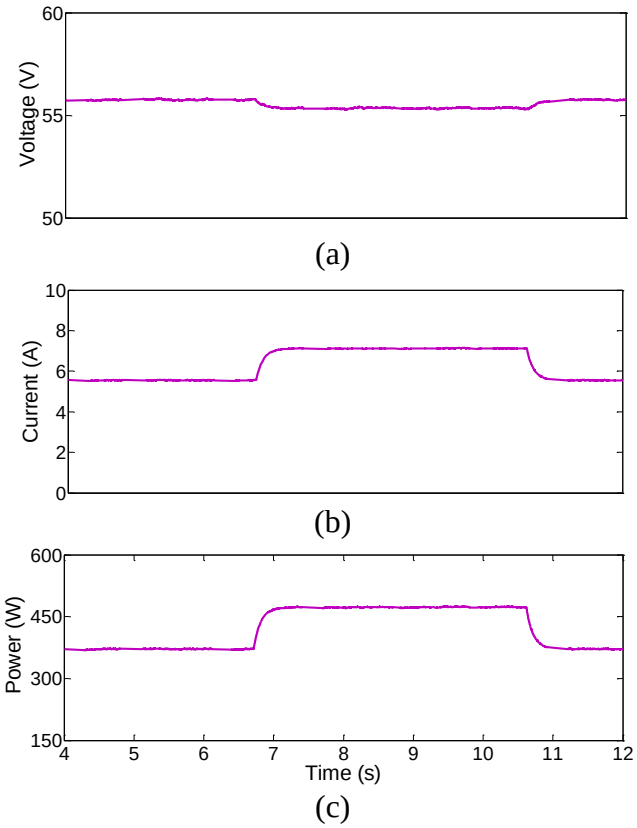

Fig. 2.12. Case 4: DG#1 performance during load change: a) Voltage at dc link, b) dc-dc converter inductor current, and c) DG output power

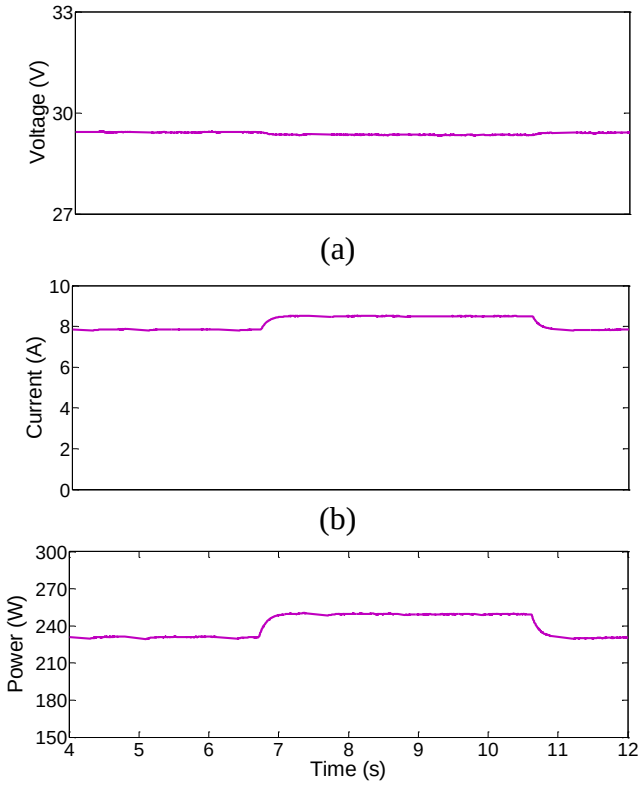

Fig. 2.13. Case 4: DG#2 performance: a) dc link voltage, b) inductor dc current, c) output power

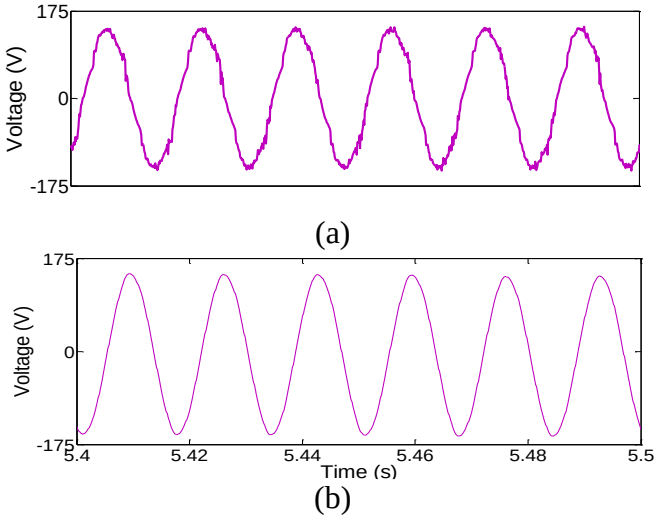

Fig. 2.14. Case 4: Voltage at Bus 1: a) Zoomed voltage, and b) filtered voltage waveform

Case 5- Cloud effect: In the second experiment, effect of a moving cloud on PV-based DG units is evaluated. The DG units are feeding the grid in normal condition while generation

capacity of one of the DG units decreases by 30% due to a passing cloud for 3s. Thus, voltage over the shaded PV panels drops to extract the maximum available power out of the panels, dc-dc converter duty cycle is also increased to maintain the dc link voltage around initial set value. On the other hand, voltage over the other DG's PV panels decreases to inject more power to the grid and compensate power loss of the other DG unit. However, dc-link voltage is kept at the initial set value due to the applied control mechanism as shown in Fig. 2.15 and Fig. 2.16.

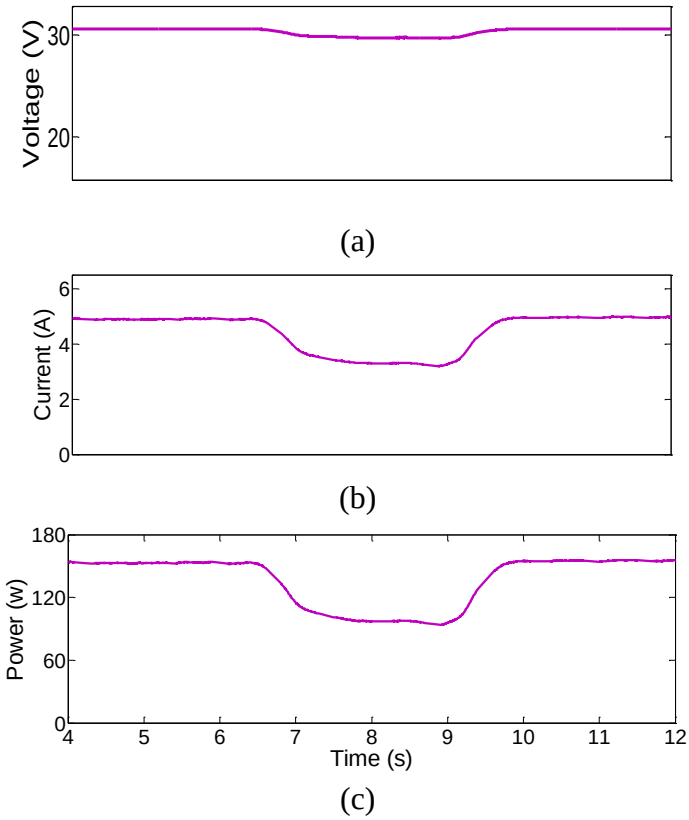

Fig. 2.15. Case 5: DG#1 performance in presence of moving cloud: a) Voltage at dc link, b) dc-dc converter inductor current, and c) DG output power

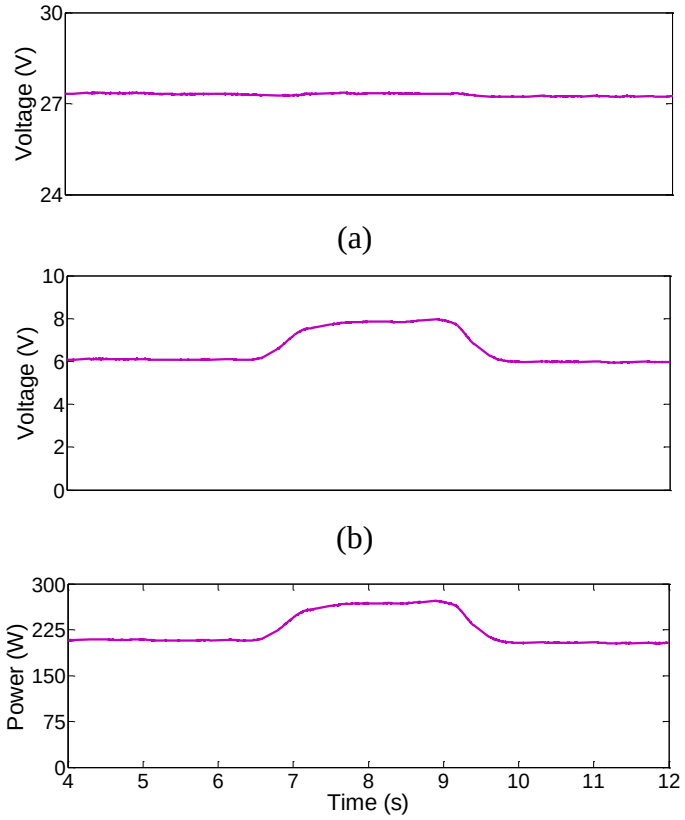

Fig. 2.16. Case 5: DG#2 performance in presence of moving cloud: a) Voltage at dc link, b) dc-dc converter inductor current, and c) DG output power

2.5 Conclusions

A novel control scheme for integrating solar power into the grid is proposed. The photovoltaic unit is connected to the grid through a dc-dc buck converter and voltage source inverter. The entire system is controlled such that the photovoltaic DG unit mimics a synchronous generator behavior in which the capacitor installed at the inverter dc link, acts similar to the synchronous generator rotating mass and maintains stability of the system in case of sudden change in the loads or the other system disturbances. An AVR-like mechanism is also introduced to the system that facilitates DG's voltage control like a synchronous machine. The proposed control scheme exhibit desired performance in stand-alone condition and in a microgrid

environment. In addition, a prototype system is implemented to validate precise operation of the control approach.

2.6 References

[1] Y. A. R. I.Mohamed and E. F. El-Saadany, "Adaptive decentralized droop controller to preserve power sharing stability of paralleled inverters in distributed generation microgrids," IEEE Trans. Power Electron., vol. 23, no. 6, pp. 2806–2816, Nov. 2008.

[2] J. C. Vasquez, J. M. Guerrero, A. Luna, P. Rodriguez, and R. Teodorescu, "Adaptive droop control applied to voltage-source inverters operating in grid-connected and islanded modes," IEEE Trans. Ind. Electron., vol. 56, no. 10, pp. 4088–4096, Oct. 2009.

[3] A. Bidram, A. Davoudi, and R. S. Balog, "Control and circuit techniques to mitigate partial shading effects in photovoltaics arrays," IEEE J. Photovolt., vol. 2, no. 4, pp. 532–546, Oct. 2012.

[4] Y. C. Chen and A. D. Garcia, "A method to study the effect of renewable resource variability on power system dynamics," IEEE Trans. Power Syst., vol. 27, no. 4, pp. 1978–1989, Nov. 2012.

[5] D. Gautam, V. Vittal, and T. Harbour, "Impact of increased penetration of DFIG-basedwind turbine generators on transient and small signal stability of power systems," IEEE Trans. Power Syst., vol. 24, no. 3, pp. 1426–1434, Aug. 2009.

[6] Anand, S., Gundlapalli, S. K., Fernandes, B. G.: 'Transformer-less grid feeding current source inverter for solar photovoltaic system', IEEE Trans. Industrial Electronics, vol. 61, no. 10, pp. 5334-5344

[7] Olivares, D. E., Mehrizi-Sani, A., Etemadi, A. H., et al.: 'Trends in microgrid control', IEEE Trans. Smart Grid, vol. 5, no. 4, pp. 1905-1919

[8] EPRI., ' Laboratory evaluation of grid-tied photovoltaic and energy storage systems ' (EPRI, Palo Alto, CA), pp. 80-85

[9] Vasquez, J. C., Guerrero, J. M., Savaghebi, M., et al.: 'Modelling, analysis, and design of stationary-reference-frame droop-controlled parallel three-phase voltage source inverters', IEEE Trans. Industrial Electronics, vol. 60, no. 4, pp. 1271-1280

[10] Vasquez, J. C., Guerrero, J. M., Luna, A., et al.: 'Adaptive droop control applied to voltage-source inverters operating in grid-connected and islanded modes', IEEE Trans. Industrial Electronics, vol. 56, no. 10, pp. 4088-4096

[11] Amelian, M., Hooshmand, R., Khodabakhshian, et al.: 'small signal stability improvement of a wind turbine-based doubly fed induction generator in a microgrid environment', Proc. 3rd Int. Conf. Computer and Knowledge Engineering, Mashhad, Iran, 2013

[12] Loh, P., Li, D., Chai, Y. K., et al.: 'Autonomous control of interlinking converter with energy storage in hybrid ac–dc microgrid', IEEE Trans. Industryl Applications, 49, (3), pp. 1374-1382

[13] Zhong, Q., Weiss, G.: 'Synchronverters: inverters that mimic synchronous generators', IEEE Trans. Industrial Electronics, 58, (4), pp. 1259-1267

[14] EPRI., 'The solar-to-battery and community energy storage project demonstrations at the solar energy acceleration center' (EPRI, Palo Alto, CA), pp. 20-25

[15] Zhong, Q., Nguyen, P., Ma, Z., Sheng, W.: 'Distributed volt/var control by pv inverters', IEEE Trans. Power Systems, 28, (3), pp. 3429-3439

[16] Malekpour, A. R., Pahawa, A.: 'A dynamic operational scheme for residential pv smart inverters', IEEE Trans. Smart Grid, 2, (99), pp. 1-10

[17] Kazemlou, S., Mehraeen, S.: 'Novel decentralized control of power systems with penetration of renewable energy sources in small-scale power systems', IEEE Trans. Energy Conversion, vol. 29, no. 4, pp. 851-861

[18] H. Saberi, and S. Mehraeen, “A Simultaneous Voltage and Frequency Control Scheme for Photovoltaic Distributed Generation Units in Small-scale Power Systems,” Proc. Energy conversion Congress & Expo (ECCE), 2017.

[19] R. C. N. Pilawa-Podgurski and D. J. Perreault, “Submodule integrated distributed maximum power point tracking for solar photovoltaic applications,” IEEE Trans. Power Electron., vol. 28, no. 6, pp. 2957–2967, Jun. 2013.

[20] G. R. Walker and P. C. Sernia, “Cascaded dc–dc converter connection of photovoltaic modules,” IEEE Trans. Power Electron., vol. 19, no. 4, pp. 1130–1139, Jul. 2004.

[21] N. Mohan, T. M. Undeland, and W. P. Robbins, Power Electronics: Converters, Applications, and Design. Hoboken, NJ, USA: Wiley, 2002.

[22] P.W. Sauer and M. A. Pai, “Power system dynamics and stability,” Stipess, Jan. 2007.

[23] Piya, P., Karimi-Ghartemani, M.: 'A stability analysis and efficiency improvement of synchronverter', Proc. Applied Power Electronics Conf. and Exposition, 2016

CHAPTER 3
STABILITY IMPROVEMENT OF MICROGRIDS USING A NOVEL REDUCED UPFC STRUCTURE VIA NONLINEAR OPTIMAL CONTROL

3.1 Introduction

Application of Flexible AC Transmission System (FACTS) devices are increasing for power quality and stability improvement in the power systems. One of the most attractive devices is Unified Power Flow Controller (UPFC) that is used in transmission systems for power flow control and transient stability improvement. Also, it can be utilized in distribution systems and micro grids to improve transient stability in addition to power flow control. In small-scale power systems and micro grids with low stored energy level, transient stability of the system is of utmost importance while various disturbances threaten stability of the system.

The UPFC consists of two main parts: shunt and series branches that are coupled together through a dc link. The shunt branch control voltage at the shunt bus through absorbing or injecting required reactive power. It also absorb the necessary active power from the grid to provide a constant voltage at the dc link. Although some dynamic variation are observable at the dc link voltage, it should be kept constant in steady state to achieve desired performance of the UPFC [1]. The series branch inject a series voltage to the power lines that is controlled for different purposes such as direct voltage injection, phase angle shifter and line impedance emulator, and automatic power flow control. The automatic power flow control can also be employed for oscillation damping and stability improvement. Thus, the injected series voltage can be controlled such that system stability is enhanced.

Different controllers can be used to determine the required series voltage based on states of the systems. Previously, linear approaches has been utilized to control the power systems [2-

7]. In those methods, the system is linearized around an operating point so that linear methods are applicable providing the system remains in a small neighborhood around the operating point that is not always a correct assumption. However, since the power systems are inherently nonlinear, nonlinear approaches are more appropriate. In addition, employing an optimal nonlinear control method minimizes the cost that is defined as a function of states and control variables [8-11]. The optimal nonlinear control method can be derived by solving the Hamilton–Jacobi–Bellman (HJB) equation.

Recently, renewable energy resources, especially Photovoltaic (PV) units, have attracted more attention as environment-friendly and abundant resource of energy. In order to integrate solar energy into the grid several methods and technologies are presented such as microinverters [12-13]. The main goal has been extracting maximum power out of the PV sources and inject it to the grid properly. Those methods are appropriate when the share of energy that comes from renewable energy resources is negligible. However, in a grid that the renewable energy resources generate a considerable share of energy Distributed Generation (DG) units should also contribute in power system control and stability [14-17].

In this paper, a small-scale micro grid that consists of DG units as the sources of energy is studied. The DG units are Photovoltaic (PV) units that are connected to the grid via dc-dc buck converters and inverters. The DG units are modeled and controlled to operate similar to a synchronous generator classical model in the power system. In order to improve the transient stability of the system, a novel reduced UPFC structure is proposed that decreases the implementation cost of the UPFC considerably. Also, an optimized mechanism is utilized for the

UPFC control to stabilize the power system by imposing the minimum cost. The minimized cost function results in lower stress on power electronics devices that increase their lifetime.

3.2 Modeling and Control of the System

The DG unit utilizes a PV source as primary source of energy. A dc-dc buck converter connects the PV unit to the inverter through a dc link capacitor. The dc-dc converter provides a constant voltage at the dc link regardless of voltage variation at the PV's output terminals. The regulated dc voltage is also used by the reduced UPFC to generate the required series voltage and inject it to the grid's power lines to enhance system stability. In this section first the DG unit modeling and control is presented and then, modeling and control of the UPFC is developed.

A. DG Unit Modeling and Control

The DG unit is modeled and controlled such that mimic behavior of a synchronous generator. Dynamic equations for the power at the dc link can be written as

$$CV_C\dot{V}_C = P_{in} - P_o \tag{1}$$

where P_{in} is the power that is injected to the capacitor from the dc-dc buck converter, P_o is the delivered power to the inverter, and V_c is the capacitor voltage. On the other hand, the inverter's delivered power to the grid will be

$$\overline{P}_e = BV_sV_1\sin(\varphi - \theta) \tag{2}$$

where B is the admittance that connect the inverter to the grid bus, V_s and φ are the voltage magnitude and phase angle at the inverter's output terminals, and V_1 and θ are the grid bus's voltage magnitude and phase angle. Neglecting the inverter's losses results in $\overline{P}_e = P_o$

In (2), the angle φ behaves similar to the stator angle δ in the synchronous generator and the inverters output power can be adjusted through changing this variable. A new variable λ is introduced to control φ in the inverter as

$$\lambda = \dot{\varphi} \tag{3}$$

λ is similar to the rotor speed (ω) in the synchronous generator. The rotor speed define its stored kinetic energy as

$$\dot{\omega} = (1/M)(P_m - P_{elec}) \tag{4}$$

where M is the moment of inertia, P_m is the input mechanical power and P_{elec} is the output electrical power. In order to relate the new variable λ to the stored energy in the dc link capacitor, it can be defined as

$$\dot{\lambda} = (1/C)(P_{in} - P_o) \tag{5}$$

Equations (3) and (5) resemble the equations of a synchronous generator classical model. In order to mimic the droop mechanism in synchronous generators, any deviation from the steady state value of λ will result in some change in the dc-dc converter's duty factor, D. This adjustment subsequently changes the operating point of the PV unit which alters its output power. Thus, any variation in λ follows by some change in the injected power which comes from the dc side that pull back the λ to its steady state value.

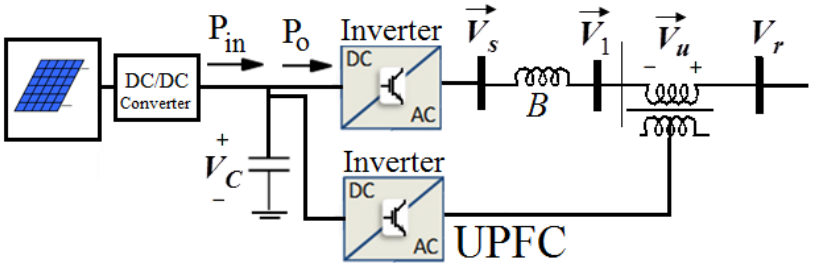

Fig. 3.1. System composed of DG and UPFC

B. Modeling and Control of the System in Presence of the UPFC

The vector diagram of the system shown in Fig. 3.1 is depicted in Fig. 3.2. The series voltage of the UPFC is composed of two components V_{up} and V_{uq}. The voltage components are considered to be proportional to the voltage at the point of connection of the UPFC. Consequently,

$$V_{uq} = V_r\beta(t),\ V_{up} = V_r\gamma(t) \tag{6}$$

where β(t) and γ(t) are two control variables. When the UPFC is taken into account, the electrical power in (2) can be written as

$$P_e = V_sV_1B\sin(\varphi-\theta) = V_sV_1B(\sin\varphi\cos\theta-\cos\varphi\sin\theta) \tag{7}$$

Based on the diagram in Fig .2,

$$\cos\theta = \frac{V_{uq}+V_r}{V_1} = \frac{(1+\beta)V_r}{V_1}$$

$$\sin\theta = \frac{V_{up}}{V_1} = \frac{(\alpha)V_r}{V_1} \tag{8}$$

Substituting (8) and (9) into (7), dynamics of the variable λ can be expressed as

$$C\dot{\lambda} = P_{in} - V_sV_rB\sin(\phi) - D\lambda + V_sV_rB\cos(\phi)\alpha(t) - V_sV_rB\sin(\phi)\beta(t) \tag{9}$$

According to the (3) and (10) the space state equations of the system will be written in the form of $\dot{x} = f(x)+g(x)u(t)$ as follows

$$\begin{bmatrix}\dot{\phi}\\ \dot{\lambda}\end{bmatrix} = \begin{bmatrix}\lambda\\ \frac{1}{C}(P_{in}-V_sV_rB\sin(\phi)-D\lambda)\end{bmatrix} + \begin{bmatrix}0 & 0\\ \frac{1}{C}V_sV_rB\cos(\phi) & -\frac{1}{C}V_sV_rB\sin(\phi)\end{bmatrix}\begin{bmatrix}\gamma\\ \beta\end{bmatrix} \tag{10}$$

By assuming the time step *T*, the system dynamic equations can be approximated in discrete-time by

$$\begin{bmatrix}\phi(k+1)\\ \lambda(k+1)\end{bmatrix}=\begin{bmatrix}\lambda T+\phi(k)\\ \frac{T}{C}(P_{in}-V_sV_rB\sin(\phi(k))-D\lambda(k))+\lambda(k)\end{bmatrix}+\begin{bmatrix}0 & 0\\ \frac{T}{C}V_sV_rB\cos(\phi) & -\frac{T}{C}V_sV_rB\sin(\phi)\end{bmatrix}\begin{bmatrix}\gamma\\ \beta\end{bmatrix} \quad (11)$$

Next, an optimal nonlinear control approach is applied to create the inputs β and γ according to the system states γ, λ.

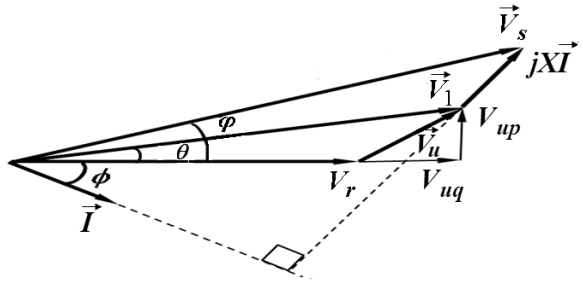

Fig. 3.2. Vector diagram of DG and UPFC

3.3 Nonlinear Optimal Controller Design

A. Control Objective

Consider the affine nonlinear state feedback discrete-time system as

$$x_{k+1}=f_k+g_ku_k \quad (12)$$

where $x_k=x(k)\in\Re^n$ is the state vector at step k, $f_k=f(x_k)$, $f(.)\in\Re^n$, $g_k=g(x_k)$, are input gain functions which are smooth and defined in a neighborhood of the origin, $u_k=u(x_k)\in\Re^m$, is the control input. Assume that $f_k+g_ku_k$ is Lipschitz continuous and there exists a control policy that can asymptotically stabilized the system. Then, the task is converted to find a control input u_k that minimizes the generalized quadratic discrete time cost function

$$V_k=\sum_{j=k}^{\infty}(Q(x_j)+u_j^TRu_j)=Q(x_k)+u_k^TRu_k+V_{k+1} \quad (13)$$

where Q and R are positive definite matrices. Meanwhile, the control policy u_k needs not only stabilizes the system, but guarantees the cost function V_k is finite, which means u_k is admissible.

Definition 1. (Admissible Control): a piecewise continuous state feedback control $u(x(k))$ is said to be an admissible control if it can not only stabilize the system but also guarantee the cost function to be finite, which means $J_k = J(x(0), u_k) < \infty$.

Note that, admissible input can make sure the system convergence, however, not all converged control input are admissible [8].

Thus, define the Hamiltonian function as

$$H(x_k, u_k) = V(f_k + g_k u_k) - V(x_k) + Q(x_k) + u_k{}^T R u_k \tag{14}$$

According to the Bellman optimality principle [9] the goal is to minimize the Hamiltonian function, and when it goes to zero, we will have discrete-time HJB equation [8]

$$V(f_k + g_k u_k^*) - V(x_k) + Q(x_k) + u_k^{*T} R u_k^* = 0 \tag{15}$$

where the optimal control policy u_k^* is the solution of (15).

By utilizing the stationary conditions, the optimal control policy u_k^* can be realized from $\partial H(x_k, u_k, w_k)/\partial u_k = 0$ as

$$u_k^* = -1/2\, R^{-1} g_k{}^T \partial V_{k+1}^* / \partial x_{k+1} \tag{16}$$

Next, by substituting (16) into (15), the HJB equation becomes

$$V_{k+1}^* - V_k^* + Q(x_k) + 1/4 \left(\partial V_{k+1}^*/\partial x_{k+1}\right)^T \times \left(-g_k R^{-1} g(x_k)^T\right) \partial V_{k+1}^*/\partial x_{k+1} = 0 \tag{17}$$

Due to the nature of partial derivatives $\partial V_{k+1}^*/\partial x_{k+1}$ and nonlinearly of the equation, it is still a challenging task to solve (17). Therefore, applying Tylor series expansion is one way to

overcome the obstacle. The difference of two adjacent cost function ΔV_k can be expanded by remaining the first and second order terms in the Taylor Series and ignoring higher order terms. In other words, higher order terms can be treated as small disturbances around the operating points. Thus, we obtain

$$\Delta V_k = V_{k+1} - V_k \approx \nabla V_k{}^T (x_{k+1} - x_k) + \frac{1}{2}(x_{k+1} - x_k)^T \nabla^2 V_k (x_{k+1} - x_k) \tag{18}$$

where ∇V_k and $\nabla^2 V_k$ are the gradient vector and Hessian matrix, respectively. Then, we obtain generalized HJB equation (19), by substituting (18) into (14).

$$Q(x_k) + u_k^T R u_k + \nabla V_k (f_k + g_k u_k - x_k) + \frac{1}{2}(f_k + g_k u_k - x_k)^T \nabla^2 V_k (f_k + g_k u_k - x_k) = 0. \tag{19}$$

with the new GHJB equation, another Hamiltonian function needs to be defined as Definition 2.

Definition 2. (Pre-Hamiltonian Function): A suitable pre-Hamiltonian function for the affine nonlinear discrete-time system (12) is defined as

$$H(x_k, V_k, u_k) = \nabla V_k (f_k + g_k u_k - x_k) + \frac{1}{2}(f_k + g_k u_k - x_k)^T \nabla^2 V_k (f_k + g_k u_k - x_k) + Q(x_k) + u_k^T R u_k. \tag{20}$$

The new optimal control policy u_k^* can be derived as

$$u_k^* = -\left[g_k^T \nabla^2 V_k g_k + 2R\right]^{-1} g_k^T \left[\nabla V_k{}^T + \nabla^2 V_k (f_k + h_k w_k^* - x_k)\right] \tag{21}$$

Now, the optimal control policy contains only the current step states x_k and get rid of x_{k+1} compare to policy (16). However, the solution of GHJB is still challenging to solve and the value function remains unknown. A successive approximation methodology is utilized by updating the approximation of GHJB and controller every iteration until it reaches to the optimal policy. In each iteration, a critic NN is applied to approximate the value function to adjust the weights vector.

B. Value Function Approximation using Neural Network

As previously discussed, the successive approximation method can be used to find the optimal control policy with modified linear GHJB (20). However, recursively solving GHJB and updating controller is impossible without knowing V_k. Before the iterative based method is implemented, V_k is approximated by NN. The NN is well known for smooth function approximation and been widely used in previous research. Thus, it is an appropriate approach for our discrete-time problem.

A nonlinear function can be approximated by a NN as

$$V_L(x) = \sum_{l=1}^{L} \omega_l \sigma_l(x) = W_L^T \bar{\sigma}_L(x) \tag{22}$$

where L is the number of neurons in the hidden layer, ω_l, are NN weights and the activation function vector $\sigma_l(x)$.Then the activation function and weights are vectored as $\bar{\sigma}_L = [\sigma_1 \quad \cdots \quad \sigma_L]^T$ and $W_L = [\omega_1 \quad \cdots \quad \omega_L]^T$. The residual error will be minimized by adjusting the weights in each iteration and be evaluated by least squares method. The solution will guarantee the lowest weights residual error.

A residual error is set as

$$GHJB\left(V_L^{(i)} = \sum_{l=1}^{L} \omega_l \sigma_l(x), u^{(i)}\right) = e_L(x) \tag{23}$$

where V_L denotes the approximation of the cost function. The weights ω_l are obtained by $\frac{\partial e_L(x)}{\partial W_L} = 0 \quad \forall \; x \in \Omega$,which means the error remains unchanged with respect to current weights. i.e.

$$\left\langle \frac{\partial e_L(x)}{\partial W_L}, e_L(x) \right\rangle = 0 \tag{24}$$

Substituting (18) and (22) into (24) yields

$$\left\langle \nabla \bar{\sigma}_L \Delta x + \frac{1}{2} \Delta x^T \nabla^2 \bar{\sigma}_L \Delta x, \nabla \bar{\sigma}_L \Delta x + \frac{1}{2} \Delta x^T \nabla^2 \bar{\sigma}_L \Delta x \right\rangle . W_L + \left\langle Q(x) + u^T R u, \nabla \bar{\sigma}_L \Delta x + \frac{1}{2} \Delta x^T \nabla^2 \bar{\sigma}_L \Delta x \right\rangle = 0 \tag{25}$$

where the terms $\nabla \bar{\sigma}_L$ and $\nabla^2 \bar{\sigma}_L$ are gradient vector and Hessian matrix of $\bar{\sigma}_L(x)$ with respect to *x*, respectively, and $\Delta x = f(x) + g(x)u(x) - x$.

By defining $\left\{ \nabla \sigma_j^T \Delta x + \frac{1}{2} \Delta x^T \nabla^2 \sigma_j \Delta x \right\}_1^L$ as $\bar{\theta}$, the current weight vector can be written as

$$W_L = -\left\langle \bar{\theta}, \bar{\theta} \right\rangle^{-1} \left\langle Q(x) + u^T R u, \bar{\theta} \right\rangle \tag{26}$$

In [8], the term $\left\langle \bar{\theta}, \bar{\theta} \right\rangle$ is shown to be full and therefore, it can be inverted, which means a unique solution W_L exists. In Hilbert space, inner product is defined as

$$\left\langle a(x), b(x) \right\rangle = \int_{\Omega} a(x) b(x) dx \approx \sum_{i=1}^{N} a(x) b(x) \delta x \tag{27}$$

Calculating the integration in (27) is computationally costly. However, by utilizing the Riemann definition of integration, it is reasonable to approximate the integration in a acceptable degree. This leads to a nearly optimal solution algorithm.

A mesh is generated on Ω, where the mesh size is δx, that is around the operation points ,(26) can be simplified as

$$W_L = -\left(X^T X\right)^{-1} XY \tag{28}$$

where *X* and *Y* are in vector form as

$$X = \left[\left(\nabla \bar{\sigma}_L \Delta x + \Delta x^T \nabla^2 \bar{\sigma}_L \Delta x / 2 \right)_{x=x_1} \quad \cdots \quad \left(\nabla \bar{\sigma}_L \Delta x + \Delta x^T \nabla^2 \bar{\sigma}_L \Delta x / 2 \right)_{x=x_p} \right]^T \tag{29}$$

$$Y = \begin{bmatrix} \left(Q(x) + u^{(i)T} R u^{(i)} \right)_{x=x_1} \\ \vdots \\ \left(Q(x) + u^{(i)T} R u^{(i)} \right)_{x=x_p} \end{bmatrix} \tag{30}$$

where p in x_p denotes the number of points of the mesh. This number increases as the mesh size is reduced. Note that activation function should be continuous and linearly independent. The mesh must generate more points compare to the order of the approximation L to guarantee the convergence. These conditions make sure $(X^T X)$ is full rank [10].

C. Successive Approximation of the Approximate HJB Equation

The successive approximation procedure starts with a selected initial admissible control policy $u_k^{(0)}$, iteratively updates the control input $u_k^{(i)}$ in a loop with index i. Then, the pre-Hamiltonian equation (20) is solved for $V_k^{(i)}$ as

$$\nabla V_k^{(i)} (f_k + g_k u_k^{(i)} - x_k) + \frac{1}{2} (f_k + g_k u_k^{(i)} - x_k)^T \times \nabla^2 V_k^{(i,j)} (f_k + g_k u_k^{(i)} - x_k) + Q(x_k) + u_k^{(i)T} R u_k^{(i)} = 0. \tag{31}$$

Next, $u_k^{(i)}$ is updated as

$$u_k^{(i+1)} = -[g_k^T (\nabla^2 V_k^{(i)}) g_k + 2R]^{-1} g_k^T \times [\nabla V_k^{(i)T} + \nabla^2 V_k^{(i)} (f_k - x_k)] \tag{32}$$

Then, next step value function is calculated by solving (31) for $V_k^{(i)}$. The iterations proceed until it converges i.e. $V_k^{(i)} = V_k^{(i+1)} = V_k^{(\infty)}$.

The convergence is proved using the following theorem.

Theorem 1. With $u_k^{(i)}$ be an admissible control for system (10) on the compact set Ω. Then, the nonlinear system $x_{k+1} = f(x_k) + g(x_k) u_k^{(i+1)}$ satisfies $V_k^{(i)} \geq V_k^{(i+1)} \geq V_k^{(*)}$ and $\lim_{i \to \infty} V_k^{(i)} = V_k^{(*)}$ where $V_k^{(*)}$ solves the approximate GHJB equation (13). Also, if $V_k^{(i)} = V_k^{(i+1)}$, then $V_k^{(i)} = V_k^*$.

An advantage of successive approximation is improved control policy according to the last step value function approximation that can guarantee the next step control policy to be admissible controller. Also, GHJB avoids the nonlinearity of the HJB that contains nonlinear partial differential equations. Now, using the successive approximation method and the approximation of GHJB by NN, the algorithm is presented as the following 5 steps:

1) Define a NN as $V = \sum_{l=1}^{L} \omega_l \sigma_l(x)$ to approximate smooth function of *V(x)*. Choose an admissible state feedback control policy $u^{(0)}$.

2) For *ith* step, find $V^{(i)}$ associated with $u^{(i)}$ to assure the approximate HJB by utilizing least square manner to find the NN weights W^i ;

3) Update the control as

$$u_k^{(i+1)} = -\left[g_k^T \left(\nabla^2 V_k^{(i)} \right).g_k + 2R \right]^{-1} g_k^T \left[\nabla V_k^{(i)} + \left(\nabla^2 V_k^{(i)} \right)(f_k - x_k) \right] \tag{32}$$

4) Find $V^{(i+1)}$ associated with $u^{(i+1)}$ to assure the approximate HJB by utilizing least square method to find the NN weights W^{i+1} ;

5) If $V^{(i)}(0) - V^{(i+1)}(0) \leq \varepsilon$, where ε is the stopping criteria as a small enough constant, then $V^* = V^{(i)}$ and stop. Otherwise, *i=i+1*, go to step2.

Once V^* is obtained, the optimal state feedback control policy will be

$$u_k^* = -\left[g_k^T \left(\nabla^2 V_k^* \right).g_k + 2R \right]^{-1} g_k^T .\left[\nabla V_k^* + \left(\nabla^2 V_k^* \right)(f_k - x_k) \right] \tag{33}$$

3.4 Test Results

The simulations are carried out in Matlab/Simulink environment. The DG unit that is equipped with the UPFC is connected to a micro grid as shown in Fig. 3.3.

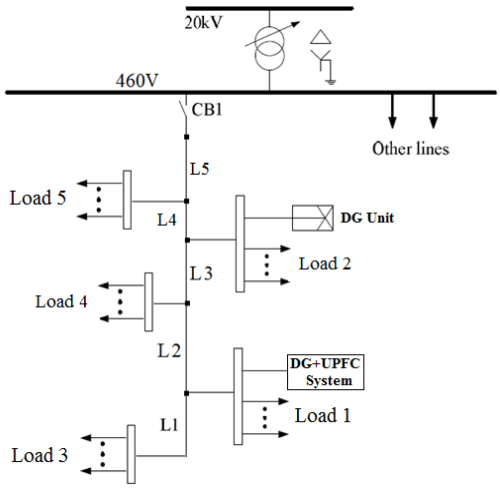

Fig. 3.3 Low voltage microgrid with DG and UPFC

Table 3.1. System parameters

Parameter	Value
- PV short circuit current	I_{sc} =9.71 A
- PV open circuit voltage	V_{oc} =39.5 V
- PV maximum power	V_{oc} =280 W
- Conv. capacitors	C_{in}=8200 µF
- Conv. Capacitor	C_{out}=8200 µF
- Conv. inductance	L=2.5 mH
- Switching frequency	f_s=10 kHz
- Filter Capacitance	C_f= 47µF
- Filter inductor	L_f= 3mH
- Line resistances	R_{Line}= 0.5 Ohm
- Line inductances	L_{Line}= 20 mH
- V_{grid}	$V_{(L-L)}$=200
- S_{base}	S_b=2KVA

In addition, the microgrid includes another PV-based DG unit, five loads at five buses of the system, and transmission lines that are modeled as series RL branches. All the system definitions are given in Table 3.1. As a case study, a fault happens on bus 1 where the DG with UPFC unit is connected. The fault occurred at t=3s and is removed after 0.2s. The presented optimal nonlinear controller regulate the injected series voltage of the UPFC in order to damp the after fault oscillations of the system. The offline training is performed in order to approximate NN weights that are used in cost function calculations. The resultant NN weights are:

W_L = [-8.4528 -0.0452 0.0018 92.5518 0.0001 0.1362 0.0000 0.0222]^T .

The proposed method can stabilize the after fault oscillations of the system's states effectively as shown in Fig. 3.4. It is also shown that when the weights are not approximated properly in the cost function, damping effect of the UPFC is deteriorated that results in more overshoot and settling time for the system states.

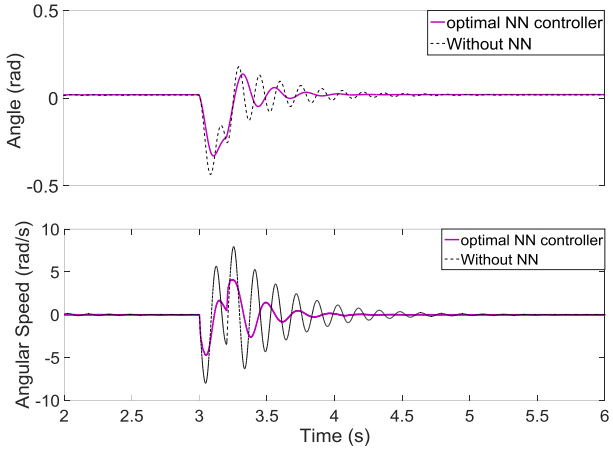

Fig. 3.4. Angle and angular speed of DG+UPFC with properly approximated and untuned weights

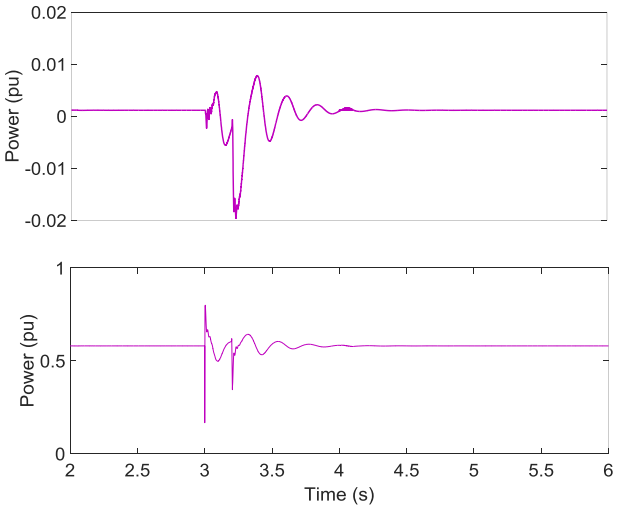

Fig. 3.5. Active power of transmision line and injected power of the UPFC

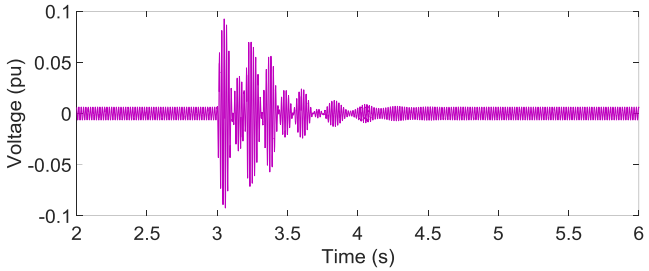

Fig. 3.6. Injected series voltage of the UPFC

The active power of the transmission line and also active power of the UPFC unit is depicted in Fig. 3.5. It is shown that the UPFC's active power is less than 2% of the nominal power. In addition, injected series voltage of the UPFC is less than 10% of the nominal voltage of the grid as demonstrated in Fig. 3.6.

Furthermore, an experimental setup is developed to test the theoretical analysis. The proposed modeling and control method is implemented using a dSPACE Microlabox control platform as shown in Fig. 3.7. The PV unit output voltage is delivered to a dc-dc buck converter. The buck converter provide a stable dc link voltage at the output. This dc voltage provide power for the three-phase inverter that feed the grid and also the inverter that generate series voltage of the UPFC unit. The LC filters are utilized to reduce voltage harmonics at the inverters output terminals. The output voltage of the main inverter feed a local load and the grid through a step up transformers. The output voltage of the UPFC inverter is also filtered, and then injected to the transmission line through the transformers that are positioned in series with the transmission lines.

The dc link voltage that is depicted in Fig. 3.8, shows voltage stability at the dc side. In addition, voltage of the grid at Bus 1 and also injected series voltage of the UPFC unit in normal condition of the microgrid is presented in Fig. 3.9 that displays stable operation of the entire system.

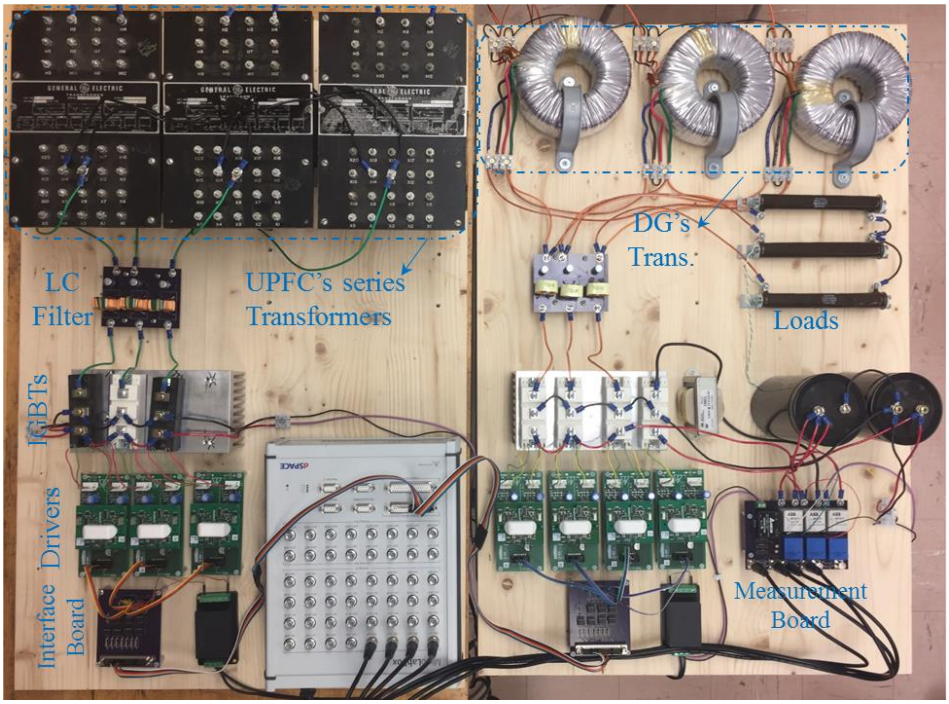

Fig. 3.7. The DG+UPFC unit that is connected to the grid at Bus1 to enhance system stability

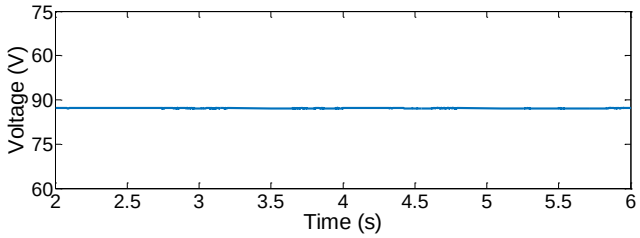

Fig. 3.8. Dc link voltage that feed both inverters of the DG+UPFC unit

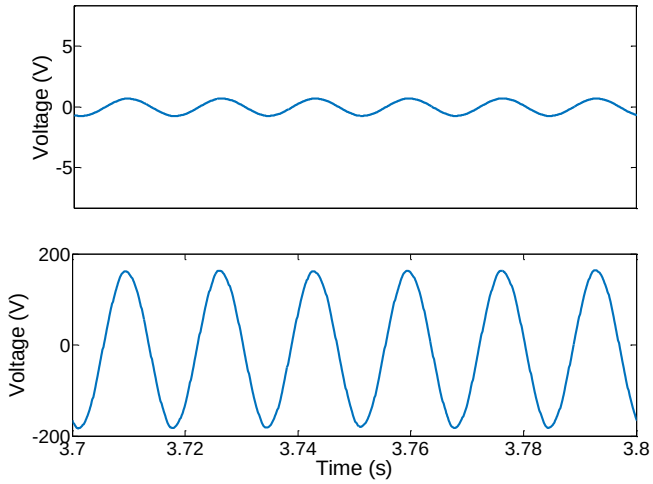

Fig. 3.9. Injected series voltage of the UPFC and grid voltage at Bus 1

3.5 Conclusion

A DG unit, composed of a PV source, dc-dc, and dc-ac converter, is modeled and controlled to behave like the classical model of a synchronous generator. Then, a novel reduced UPFC structure is presented and governed via an advanced optimal nonlinear control method to stabilize the DG unit in the micro grid environment. The proposed scheme could damp the system oscillations effectively. Although the proposed method is applied to the reduced UPFC structure in a micro grid environment, the scheme is applicable to traditional UPFCs in the power systems. The novel model is implemented for the first time and experiments are carried out that demonstrate the control scheme efficacy.

In this section, the dynamical model along with the control mechanism of the DERs is represented. Though the proposed modeling and controller design can be applied to a variety of DERs, specific attention is paid to photovoltaic source here to address the low-inertia distribution systems and micro grids. Fig. 3.1 shows the interconnected dc grid comprising N buses with n DER buses and N-n load buses.

3.6 References

[1] C. D. Schauder, L. Gyugyi, et al., "Operation of the Unified Power Flow Controller (UPFC) under Practical Constraints," IEEE Transactions on Power Delivery, vol. 13, no. 2, pp. 630-639, Apr. 1998.

[2] C. Li-Jun, and I. Erlich, "Simultaneous Coordinated Tuning of PSS and FACTS Damping Controllers in Large Power Systems," IEEE Transactions on Power Systems, vol. 20, no. 1, pp. 294 – 300, Feb. 2005.

[3] B. C. Pal, "Robust Damping of Interarea Oscillations with Unified Power-flow Controller," IEE Proceedings-Generation, Transmission, and Distribution, vol. 149, no. 6, pp. 733-738, Nov. 2002.

[4] N. Yang, Q. Liu., and J.D. McCalley, “TCSC Controller Design for Damping Interarea Oscillations,” IEEE Transactions on Power Systems, vol. 13, no. 4, pp. 1304 – 1310, Nov. 1998.

[5] J. Guo, “Decentralized Control and Placement of Multiple Unified Power Flow Controllers,” Missouri University of Science and Technology, PhD Dissertation, pp. 40-67, 2006.

[6] C.T. Chang, and Y. Y. Hsu, “Design of UPFC Controllers and Supplementary Damping Controller for Power Transmission Control and Stability Enhancement of a Longitudinal Power System,” IEE proceedings, Generation, Transmission, and Distribution, vol. 149, no. 4, pp. 463-471, Jul. 2002.

[7] J. Guo, M. L. Crow, and J. Sarangapani, “An Improved UPFC Control for Oscillation Damping,” IEEE Transactions on Power Systems, vol. 24, no. 1, pp. 288-296, Feb. 2009.J. Clerk Maxwell, A Treatise on Electricity and Magnetism, 3rd ed., vol. 2. Oxford: Clarendon, 1892, pp.68–73.

[8] Z. Chen and S. Jagannathan, “Generalized Hamilton–Jacobi–Bellman formulation-based neural network control of affine nonlinear discrete-time systems,” IEEE Trans. Neural Networks., vol. 10, no. 1, pp. 90–106, 2008

[9] F. L. Lewis and V. L. Syrmos, Optimal Control, 2nd ed. Hoboken, NJ:Wiley,1995.

[10] Nazaripouya, H., and S. Mehraeen. "Control of UPFC using Hamilton-Jacobi-Bellman formulation based neural network." Power and Energy Society General Meeting, 2012.

[11] H. Nazaripouya, and S. Mehraeen, “Modeling and Nonlinear Optimal Control of Weak/Islanded Grids Using FACTS Device in a Game Theoretic Approach,” IEEE Transactions on Control Systems Technology, vol. 24, no. 1, pp. 158-171, Jan. 2016.

[12] S. M. Tayebi, C. Jourdan, and I. Batarseh, “Dynamic Dead Time Optimization and Phase-Skipping Control Techniques for Three-Phase Micro-Inverter Applications,” IEEE Transactions on Industrial Electronics, vol. 63, no. 12, pp. 7523-7532, Dec. 2016.

[13] S. M. Tayebi, and I. Batarseh, “Analysis and Optimization of Variable-Frequency Soft-Switching Peak Current Mode Control Techniques for Microinverters,” IEEE Transactions on Industrial electronics, vol. 33, no. 2, pp. 1644-1653, Feb. 2017.

[14] H. Saberi, and S. Mehraeen, “A Simultaneous Voltage and Frequency Control Scheme for Photovoltaic Distributed Generation Units in Small-scale Power Systems,” Proc. Energy Conversion Congress & Expo (ECCE), 2017.

[15] H. Davarikia, F. Znidi, MR. Aghamohammadi, K. Iqbal, “Identification of coherent groups of generators based on synchronization coefficient,” Proc. Power and Energy Society General Meeting (PESGM), 2016.

[16] F. Znidi, H. Davarikia, K. Iqbal, “Modularity clustering based detection of coherent groups of generators with generator integrity indices,” Proc. Power and Energy Society General Meeting (PESGM), 2017

[17] H. Davarikia, M. Barati, F. Znidi, K. Iqbal, “Real-Time Integrity Indices in Power Grid: A Synchronization Coefficient Based Clustering Approach,” Proc. Power and Energy Society General Meeting (PESGM), 2018

VITA

Hossein Saberi received the B.Sc. degree in electrical engineering from Isfahan University of Technology, Isfahan, Iran, and the M.Sc. degree from University of Tabriz, Tabriz, Iran, in 2009 and 2013 respectively. He is pursuing his Ph.D. in electrical engineering in Louisiana State University, Baton Rouge, LA, USA, with anticipated graduation in May 2018. His research interests include power electronics applications in ac and dc microgrids, decentralized control, electric machinery, and electric drive systems.